

University of Mississippi

eGrove

Honors Theses

Honors College (Sally McDonnell Barksdale
Honors College)

Spring 5-7-2022

Analysis of Hemp Fiber Reinforced Polylactide Composite Under High Strain-Rate

Benjamin Rhoads

Follow this and additional works at: https://egrove.olemiss.edu/hon_thesis



Part of the [Polymer and Organic Materials Commons](#)

Recommended Citation

Rhoads, Benjamin, "Analysis of Hemp Fiber Reinforced Polylactide Composite Under High Strain-Rate" (2022). *Honors Theses*. 2564.

https://egrove.olemiss.edu/hon_thesis/2564

This Undergraduate Thesis is brought to you for free and open access by the Honors College (Sally McDonnell Barksdale Honors College) at eGrove. It has been accepted for inclusion in Honors Theses by an authorized administrator of eGrove. For more information, please contact egrove@olemiss.edu.

ANALYSIS OF HEMP FIBER REINFORCED POLYLACTIDE COMPOSITE UNDER
HIGH STRAIN-RATE

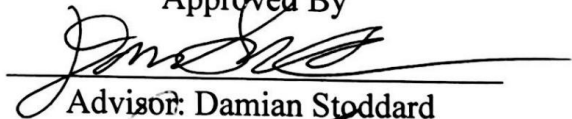
By
Benjamin Rhoads


A thesis submitted to the faculty of The University of Mississippi in partial fulfillment of
the requirements of the Sally McDonnell Barksdale Honors College.


Oxford, MS

14 April, 2022

Approved By


Advisor: Damian Stoddard


Reader: Dr. Tejas Pandya


Reader: Dr. Arunachalam Rajendran

© 2022

Benjamin Mullins Rhoads
ALL RIGHTS RESERVED

DEDICATION

This thesis is dedicated to my amazing and beautiful fiancée, Dasana. I am thrilled to get to spend the rest of my life with you. I love you so much.

ACKNOWLEDGEMENTS

The author would like to thank and acknowledge: Mr. Damian Stoddard, for guidance and assistance during this project; the undergraduate research students who helped with this project; the Mechanical Engineering Department at the University of Mississippi, for providing everything necessary to excel as an engineer; the University of Mississippi, for creating an atmosphere where everyone is pushed to their limits; 3D-Fuel, for providing the materials to test; and finally, my friends and family, who support me in everything I do. I would not be where I am today without every one of you.

ABSTRACT

BENJAMIN MULLINS RHOADS: Analysis of Hemp Fiber Reinforced Polylactide Composite Under High Strain-Rate

The introduction of hemp fibers into a polylactide (PLA) matrix creates a hemp fiber-reinforced composite with 10% hemp fibers and 90% PLA. Natural fibers are becoming a popular alternative to synthetic fibers since they are environmentally friendly, and hemp-fibers are becoming used more often as the demand for natural fibers increased. A Split-Hopkinson Pressure Bar was used to test this composite against a control group using elastic wave propagation theory. Strain gauges were mounted on the incident and transmission bars of the SHPB to measure the propagation of the wave that caused the strain in the sample, which were used to calculate the values desired. Each material was tested under three different pressures of the gas chamber in the SHPB to yield a range of strain-rates: 30, 40, and 50 psi. The ultimate compressive strength, damage initiation energy, and damage propagation energies were analyzed to conclude whether the hemp fibers had an impact on the performance on the PLA matrix. The range of strain-rates in the control group and hemp composite group was 1807-2800 /s and 2112-2925 /s, respectively, and the ultimate compressive strengths were 112.5-128.8 MPa and 72.8-110.8 MPa, respectively. Subsequently, the total specific energy of the control group and hemp composite group ranged from 24.3-35.4 kJ/kg and 19.84-25.2 kJ/kg, respectively. These results showed that the introduction of hemp fibers into the PLA matrix caused the compressive strength and specific energy to decrease significantly. The conclusion was that the hemp fiber-reinforced PLA composite showed lower compressive strength and specific energy under high strain-rates than PLA with no fibers added.

TABLE OF CONTENTS

DEDICATION	iii
ACKNOWLEDGEMENTS	iv
ABSTRACT	v
TABLE OF CONTENTS	vi
LIST OF FIGURES	viii
LIST OF TABLES	x
LIST OF ABBREVIATIONS	xi
INTRODUCTION	1
Purpose	1
Background Information and Research	2
High Strain-rate Testing – Methods and Analysis	4
High-Speed Video Capturing	7

Analysis Calculations	7
Hypothesis	11
Procedure	12
ANALYSIS	15
MATLAB Analysis	15
Digital Image Correlation Analysis	17
RESULTS AND DISCUSSION	22
Control PLA Group Results	22
Hemp-PLA Group Results	25
Comparisons	27
CONCLUSIONS	39
LIST OF REFERENCES	40

LIST OF FIGURES

Figure 1	Diagram of Left Side of SHPB	4
Figure 2	Diagram of Right Side of SHPB	4
Figure 3	Sample Set-up in SHPB	5
Figure 4	Camera and Lights Set-up in SHPB	6
Figure 5	Wheatstone Bridge Configurations - (a) basic; (b) quarter-bridge; (c) half-bridge; (d) full-bridge [10]	6
Figure 6	Damage Initiation vs. Damage Propagation Diagram	11
Figure 7	Orientation of Sample in SHPB	13
Figure 8	MATLAB Primary Display Interface	15
Figure 9	Calculated Plots from Primary MATLAB Execution	16
Figure 10	MATLAB Final Display Interface	17
Figure 11	ProAnalyst Calibration	18
Figure 12	ProAnalyst Line Tracking	19
Figure 13	Strain vs. Time - Strain Gauge/DIC Analysis – 1917 /s, Control Group	19
Figure 14	Strain vs. Time - Strain Gauge and DIC Analysis – 2185 /s, Control Group	20
Figure 15	Strain vs. Time - Strain Gauge and DIC Analysis – 2626 /s, Control Group	20
Figure 16	Strain vs. Time - Strain Gauge and DIC Analysis – 2228 /s, Hemp Group	20
Figure 17	Strain vs. Time - Strain Gauge and DIC Analysis – 2354 /s, Hemp Group	21
Figure 18	Strain vs. Time - Strain Gauge and DIC Analysis – 2775 /s, Hemp Group	21
Figure 19	Stress vs. Strain - Control Group	22
Figure 20	Stress vs. Strain – 1821-2060 /s – Control	23

Figure 21	Stress vs. Strain – 2165-2221 /s – Control	24
Figure 22	Stress vs. Strain – 2447-2795 /s – Control	24
Figure 23	Stress vs. Strain - Hemp-PLA Group	25
Figure 24	Stress vs. Strain – 2125-2314 /s - Hemp PLA	26
Figure 25	Stress vs. Strain – 2369-2494 /s - Hemp PLA	26
Figure 26	Stress vs. Strain – 2827-2948 /s - Hemp PLA	27
Figure 27	Stress vs. Strain - Hemp (Orange) and Control (Blue)	28
Figure 28	Ultimate Compressive Strength vs. Strain-rate	29
Figure 29	Ultimate Compressive Strength vs. SHPB Pressure	29
Figure 30	Ultimate Compressive Strength	30
Figure 31	Specific Energy vs. Strain-rate	31
Figure 32	Total Specific Energy vs. SHPB Pressure	32
Figure 33	Total Specific Energy	32
Figure 34	Damage Initiation Energy vs. Strain-rate	33
Figure 35	Damage Initiation Energy	34
Figure 36	Damage Propagation Energy vs. Strain-rate	34
Figure 37	Damage Propagation Energy	34

LIST OF TABLES

TABLE 1	Ranges of Main Results - Control vs. Hemp-PLA	35
---------	---	----

LIST OF ABBREVIATIONS

PLA	Poly lactide or Polylactic Acid
SHPB	Split-Hopkinson Pressure Bar
ABS	Acrylonitrile butadiene styrene
HPV	Hyper-vision
MATLAB	Matrix Laboratory
DIC	Digital Image Correlation

INTRODUCTION

Purpose

The purpose of this study was to analyze the effects on polylactide (PLA) 3D printing filament with hemp fibers, creating a hemp fiber-reinforced PLA composite. An analysis was performed on the response of the samples under three ranges of strain-rates and compared to tests done to PLA filament-based samples under similar strain-rates and similar print settings. These tests were conducted to determine if there was a difference in the performance of hemp-fiber PLA composites compared to 100% PLA under high strain-rates.

Hemp has been used more and more recently as it can be used in many applications, and is sustainable and biodegradable, which has minimal impact on the Earth. The fibers can be used to make composites, fabrics, ropes, canvas, and other materials. Replacing a portion or all plastic materials with hemp fibers allows the material to have less negative impact on the planet, and if the performance and price of the material is not compromised, then hemp-based materials will continue to be pursued. Understanding the performance of hemp fiber-reinforced PLA composites under high strain-rates is essential because materials perform differently at various strain-rates [1].

Background Information and Research

Hemp does not require herbicides or pesticides and grows more abundantly than other common crops, like corn, meaning it is an environmentally and economically safe alternative to other 3D printing filaments, like PLA and acrylonitrile butadiene styrene (ABS), which are the most common filaments and do not have reinforcements. Hemp fibers are produced using strictly the cellulose extracted from the hemp plant, as opposed to plastics, which require using petroleum to produce, which is harmful to the environment. Hemp is currently being used for various applications, including press-molded interior panels in automobiles, geotextiles, thermal insulation mats used in construction, and many other potential future applications. [2].

This hemp-fiber PLA composite filament is made with over 90% PLA, which is compostable, and the other portion is comprised of hemp fibers [3]. Hemp fibers are emerging as a biodegradable, environment-friendly material, that can replace many other materials that are harmful to the environment while still retaining the same material properties. Many composites have been developed that are reinforced using natural fibers, including hemp. This fiber, along with other plant-based fibers, are becoming a great alternative to glass fibers being used as the reinforcement [4].

There have been some studies on the response of 3-D printed materials under high strain-rates. For example, Chaudhry, S. et. al. performed both quasi-static and high-strain-rate loads on 3-D printed thermoplastic polyurethane, examining the effects of various ways of printing the material, such as the infill pattern, infill percentage, layer height, and orientation were adjusted, and the results were analyzed. The results showed that the compressive strength of the 3D-printed samples increased as the strain-rate increased from

2000 /s to 4500 /s. The orientation also had an impact on the compressive strength. There was about a 33% increase in the compressive strength when the load was applied collinearly to the plane of the sample compared to when the load was perpendicular to the sample planes. [5].

High-strain-rate compression has been performed on hemp-fiber composites with an epoxy resin and were compared to their performance under quasi-static compression. There were four composites tested, each with different percent weights of hemp fibers: 1%, 2%, 5%, and 10%. All the composite's ultimate compressive strengths were about double the compressive strengths of the composites under quasi-static compression [hemp-fiber compression]. This is due to strain hardening, which is where the strength of a composite increases as the strain-rate increases [6][7]. The expectation is that the hemp fibers in the PLA will contribute to strain hardening and will contribute to hemp-fiber reinforced PLA having a higher compressive strength than the 100% PLA filament.

Strain hardening occurs in many composites, including hemp fiber-reinforced composites. In a study, the maximum compressive strength of a hemp fiber-reinforced vinyl ester thermoset composite increased from 102 MPa to 239 MPa as the strain-rate increased from 629 /s to 2258 /s [8]. However, in this study, the hemp fiber-reinforced composite showed significant decrease in strain hardening as the strain-rate reached higher values. When the strain-rate went from 1511 /s to 2258 /s, the maximum compressive strength went from 232 MPa to 239 MPa, which is just a 3% increase. The maximum compressive stress increased at a rate directly proportional to the strain-rate until this point, where it essentially plateaued [9]. In this experiment, the goal is to see if similar strain hardening occurs when the hemp fibers are printed in a PLA matrix.

High Strain-rate Testing – Methods and Analysis

Testing a material as it undergoes a high strain-rate is an integral part of fully understanding its response to impact. It is especially useful for understanding how the energy absorption and stress-strain curve is similar or different to the material under quasi-static and low velocity testing. The information from this method of testing can give a more accurate picture of how a material will react to high-velocity impacts in the real world. The Split Hopkinson Pressure Bar (SHPB) was used to perform high strain-rate testing. Figures 1 and 2 below show the front and rear parts of the SHPB, respectively.

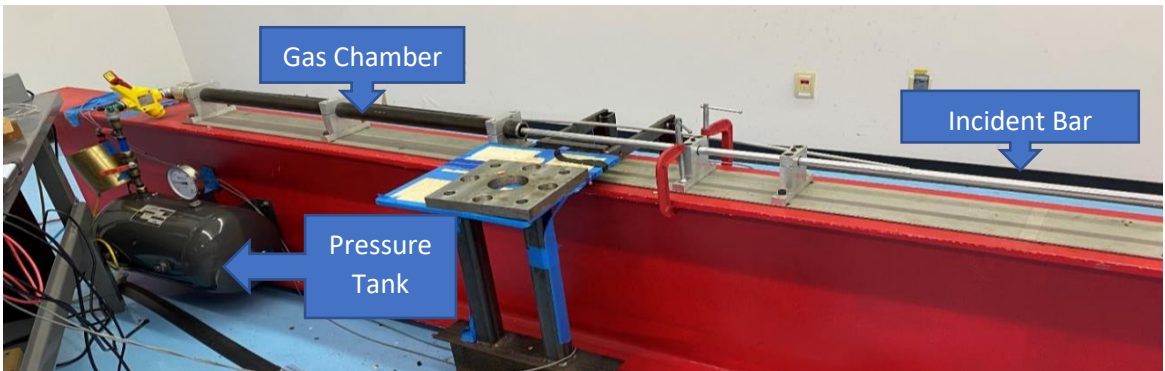


Figure 1 - Diagram of Left Side of SHPB

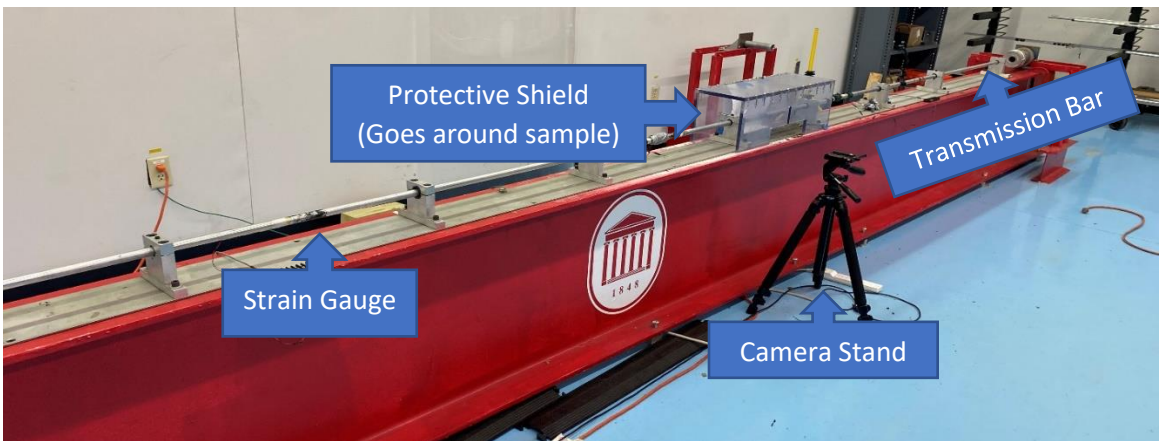


Figure 2 - Diagram of Right Side of SHPB

From left to right, the gas chamber is the first component, with the striker rod inside the gas chamber, then the incident bar is against the end of the gas chamber, and the sample is against the other end of the incident bar, which can be seen in Figure 3. The transmission bar is against the other side of the sample, and the shock absorber is on the other side of the transmission bar. The camera stand is on the side of the SHPB, where the camera and lights are directed towards the sample. The camera and strobe lights setup are shown in Figures 3 and 4. Pressurized gas is built up in the chamber which is released all at once into the striker rod, which strikes the incident bar. The incident bar then compresses the sample into the transmission bar, which strikes into the shock absorber.

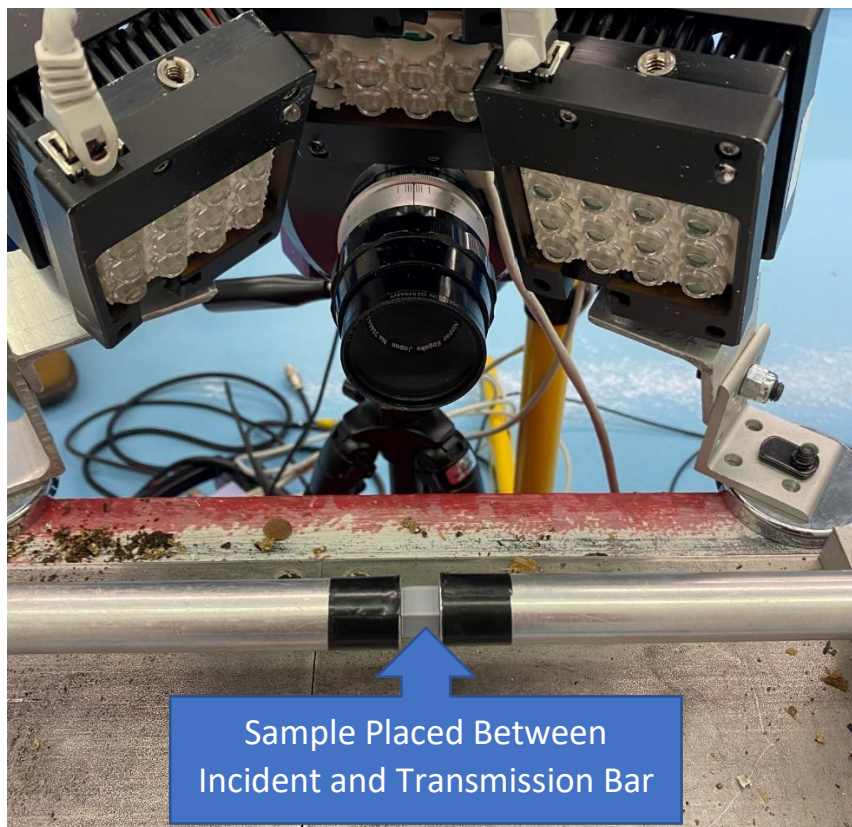


Figure 3 - Sample Set-up in SHPB

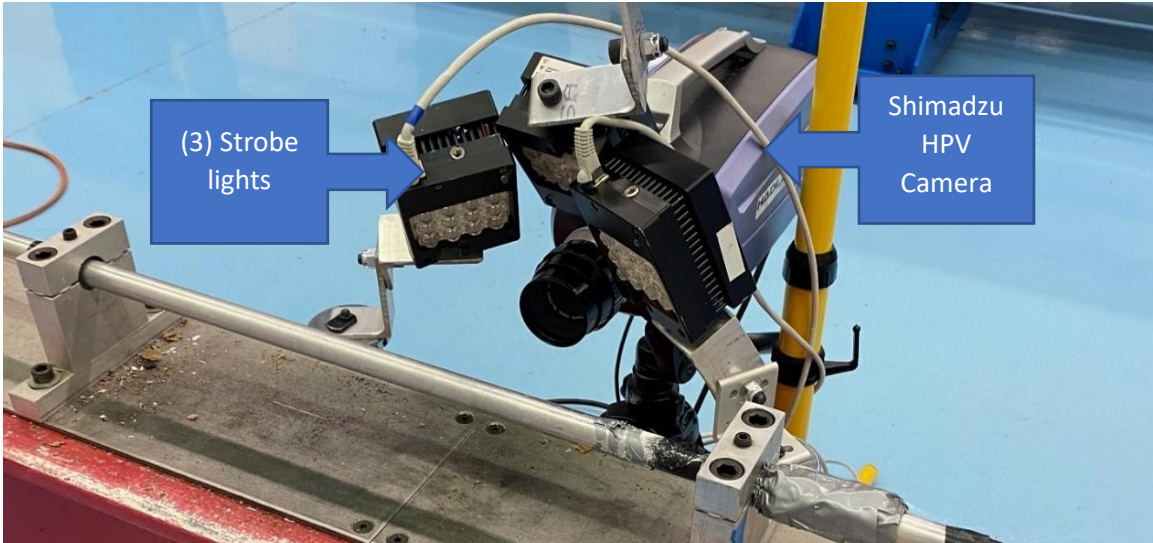


Figure 4 - Camera and Lights Set-up in SHPB

A strain gauge constructed using a Wheatstone bridge circuit is placed on the incident and transmission bar, which measures the strain that travels through the bars as it goes through the incident bar, the sample being tested, the transmission bar, and the portion that is reflected from the sample back into the incident bar. Figure 5 below shows the various Wheatstone bridge configurations of strain gauges.

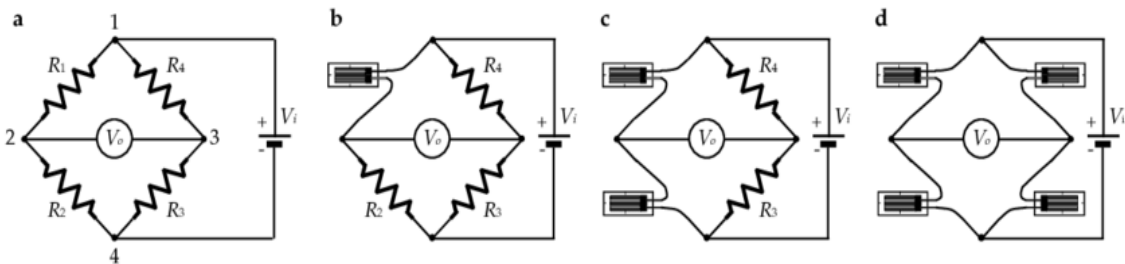


Figure 5 - Wheatstone Bridge Configurations - (a) basic; (b) quarter-bridge; (c) half-bridge; (d) full-bridge [10]

Diagram (c) shows the quarter-bridge Wheatstone configuration, where one of the four resistors in the circuit are variable resistors. Two gauges are used, one on each side of the bars, so that if there is torsion or bending in the bars, the added tension and compression

on opposite sides of the bar would cancel out, and the overall change in length of the resistor is more accurate. A voltage is input into the circuit, and when the variable resistor changes length, the output voltage changes, and this change is used to calculate the strain of the bar. This signal is sent to a signal amplifier, which is read by a picoscope. The picoscope displays the result in the form of voltage versus time. This, along with other measured property values of the components of the system, is all that is needed to perform the analysis on the tested sample.

High-Speed Video Capturing

One requirement of this procedure was to capture a video of the sample as it undergoes strain. This requires recording an event that lasts less than 1 millisecond. Therefore, the frame rate of the video must be extremely high. A Shimadzu HPV video camera was used, which has a fixed camera resolution of 312 x 260 pixels and can capture up to 1 million frames per second. For this procedure, the compression of the sample was recorded at a frame rate of 250,000 frames per second. Using this video with digital image correlation (DIC) software from ProAnalyst software, the strain of the sample was observed and compared to the strain of the sample calculated using 1D elastic wave theory. This was to confirm the strain-rate and strain for conventional analysis.

Analysis Calculations

The main result in this test is the stress-strain relation of the sample. The first step of this analysis is to calculate the modulus of elasticity of the incident and transmission

bars used in the test. Equations 1 through 7 are shown below, which explain how the data from this procedure was analyzed [11]. Equation 1 below shows that the wave speed is needed, which is calculated using the distance between the two strain gauges on each beam and the time it takes between pulses.

$$\text{Wave speed } (v) = \frac{\text{distance between two strain gauges}}{\text{time between pulses}} \quad (1)$$

The wave speed represents how fast stress travels through the bars in the Split Hopkinson Pressure Bar. The other value needed is the density of the bar, which is then multiplied by the square of the wave speed to calculate the modulus of elasticity of the bar, shown in Equation 2.

$$\text{Modulus of Elasticity } (E) = v^2 * \rho \quad (2)$$

In this Equation, v is the wave speed and ρ is the density of the bar. Next, the strain in the bar was calculated, using the strain gauges. When a voltage is sent through a strain gauge, the voltage output is a function of the resistances of the strain gauge. Equation 3 shows this relation.

$$\text{Voltage Output} = \frac{R_1 R_3 - R_2 R_4}{(R_1 + R_2)(R_3 + R_4)} * V_{in} \quad (3)$$

In a quarter bridge circuit, R_1 is the only resistor that changes length, R_2 , R_3 , and R_4 are non-changing resistors, and V_{in} is the input voltage. The voltage output is displayed on the oscilloscope. Equation 4 below shows how this reading is used to calculate the strain in the bar.

$$Strain (\varepsilon) = V_{out} * \frac{\Omega_g}{\left(\frac{V}{\varepsilon}\right) * GF * (\Omega_g + \Omega_c)} \quad (4)$$

In this equation, V_{out} is the voltage read by the oscilloscope, Ω_g is the gauge resistance, GF is the gauge factor, and Ω_c is the resistance of the calibration resistor. V/ε is the voltage per strain and represents the amount of strain per voltage change in the Wheatstone bridge.

In this setup, 1 mV corresponds to 1 micro strain, which is a $\left(\frac{V}{\varepsilon}\right)$ of 0.001.

Stress in the sample is then calculated, and since the sample is essentially a part of a continuous system of the incident bar, sample, and transmission bar, the force is equal through the whole system. Therefore, the stress in the sample is equal to the stress in the transmission bar ($\sigma_\tau = E_\tau * \varepsilon_\tau$) multiplied by the ratio of the cross-sectional area of the bar (A_{bar}) to the cross-sectional area of the sample (A_{sample}), as seen in Equation 5.

$$\sigma_{sample} = \frac{A_{bar}}{A_{sample}} * E_\tau \varepsilon_\tau \quad (5)$$

The stress from the transmission bar is used instead of the incident bar because part of the elastic wave that the striker rod transmits into the incident bar is reflected by the sample due to the bar and sample being different materials and cross-sectional areas. The remaining portion of the elastic wave travels through the sample and the transmission bar, meaning the force measured in the transmission bar is equal to the force that is applied to the sample, which allows the stress in the sample to be calculated as previously shown in Equation 5.

Next, the strain-rate of the sample is calculated, which is used to determine if the stress-strain relation varies based on the sample's strain-rate. The strain-rate ($\dot{\epsilon}$) of the sample is calculated using Equation 6 below.

$$\dot{\epsilon}_{sample} = -2 * \frac{v_{incident}}{l_{sample}} * \epsilon_{reflected} \quad (6)$$

In this equation, $v_{incident}$ is the wave speed in the incident bar, l_{sample} is the length of the sample, and $\epsilon_{reflected}$ is the strain in the reflected bar. Finally, the energy absorbed by the sample was calculated. The energy density is calculated by finding the area under the stress-strain curve and is found in units of Joules per cubic meter. This energy is referred to as the energy density, as it is in units of joules per unit volume. This value is divided by the density of the sample to get the specific energy, which is in units of joules per kilograms. This value can be compared for all samples because it takes away any variation in energy absorbed due to a difference in the mass of the sample. Equation 7 below shows how to calculate the specific energy of the sample.

$$Specific\ Energy = \frac{(change\ in\ strain) * (stress)}{density} \quad (7)$$

The specific energy is split into two parts: damage initiation and damage propagation energy. The former represents the energy absorbed by the sample before it reaches its ultimate compressive strength, while the latter represents the energy absorbed by the sample after it has reached its ultimate compressive strength. The visible compression can be seen before failure; then, after failure, the damage becomes visible. Figure 6 below illustrates these two values.

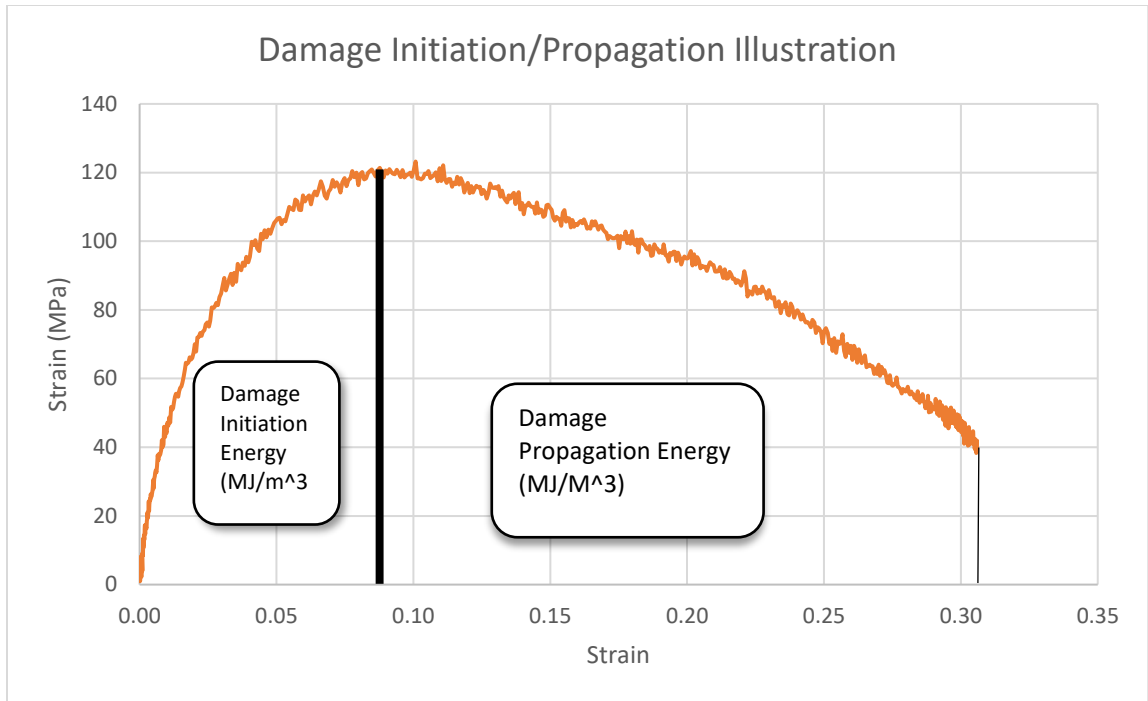


Figure 6 - Damage Initiation vs. Damage Propagation Diagram

Hypothesis

The response of hemp-infused PLA was compared to that of 100% PLA under three high strain-rates. A Split Pressure Hopkinson Bar was used to conduct this test, and the results were gathered and analyzed to formulate the stress-strain curve for each 3-D printed material at each strain-rate. It is expected that the hemp fibers in the PLA will allow the material to handle higher compressive strengths and have a higher energy density than the 100% PLA material under high strain-rates.

Procedure

Two materials were tested, the first containing 100% PLA, the second comprised of 90% PLA and 10% hemp fiber. In the procedure, each material was tested 3 times at gas chamber pressures of 30, 40, and 50 psi, for a total of 18 samples tested. The filament was obtained from a company titled 3D-Fuel (United States, North Dakota, 2022). A spool of 1.75mm-diameter filament of the hemp-fiber composite was obtained, and a spool of 100% PLA was obtained for investigation in this study. The samples were printed using a QIDI X-MAX 3-D Printer, with the extruder temperature at 190 degrees Celsius and the base plate temperature at 60 degrees Celsius. The print speed of the extruder nozzle to build the sample was a rate of 30 mm/s. The dimensions of the cube were 10mm x 10mm x 10mm, and the actual measurements, along with the mass, were measured to the nearest ten thousandth of a gram and the nearest hundredth of a millimeter. Once the samples were printed, they were subjected to high strain-rate compressive loading using a SHPB.

To capture video of the sample being compressed at a high strain-rate, the Shimadzu HPV video camera was used. The camera was positioned within one foot of the sample, which was covered by a protective shield, and the lens was adjusted so the sample was in focus. Because the camera measures at a very high frame rate, it requires extra light to be on whatever is being recorded. Therefore, multiple LEDs needed to be directed onto the sample to provide enough light for the video recorded at the specific frame rate to be visible. When the SHPB fired, a trigger was set off in the software of the Shimadzu camera, which began recording the video of the sample. This video was then saved to the computer and used by the Digital Image Correlation software to measure strain-rate.

To provide the pressure needed to propel the striker rod into the incident bar, a pressure was needed at the beginning of each test. The chamber was filled with 30, 40, and 50 psi of air before each test, to produce strain rates between 1807 and 2925 /s. The striker rod was then slid into the back of the chamber, and the incident bar's open end was placed in line with the opening of the chamber that housed the striker rod. The sample was then placed between the incident bar and the transmission bar, with the sample orientation as shown below in Figure 7. As seen in Figure 7 below, the top and bottom of each sample are both touching the ends of the incident and transmission bars, so the stress wave travels perpendicular to the planes in the sample. This ensures that each sample reacts in a similar way, since 3D-printed materials are printed one layer at a time, the orientation of the sample was kept constant.

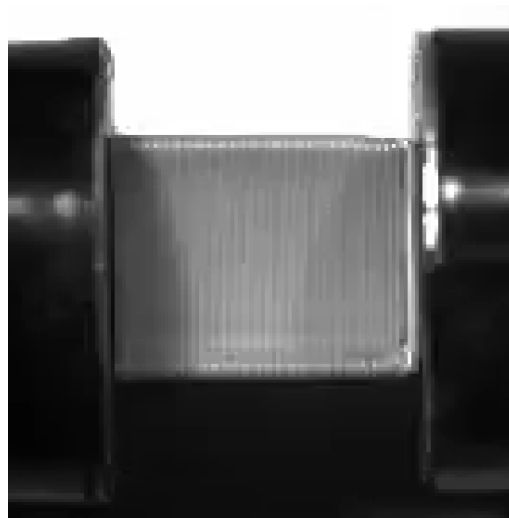


Figure 7 - Orientation of Sample in SHPB

The pressure was released, causing the striker rod to impact the incident bar, sending an elastic wave through the bar and into the sample. A portion of the wave was reflected into the incident bar, and the rest traveled through the sample and the transmission

bar, meaning the same wave that traveled through the sample traveled through the transmission bar. The data gathered from the strain gauge on the transmission bar is used to obtain the force that is experienced in the sample as well as the stress. The reflected wave that is recorded by the strain gauge on the incident bar is used to calculate the strain-rate in the sample, which can be integrated to find the strain at a given time. Since the stress in the sample was calculated as a function of time, the stress and strain could be coupled together based on time, and a stress-strain curve could be formulated.

ANALYSIS

MATLAB Analysis

Using an open-source MATLAB script, the following interface in Figure 8 below is shown. The first step, shown in this display, is to match the incident, transmission, and reflected waves together so they all begin as close to the origin as possible. Theoretically, when the reflected wave is subtracted from the incident wave, it should be equal to the transmission wave.

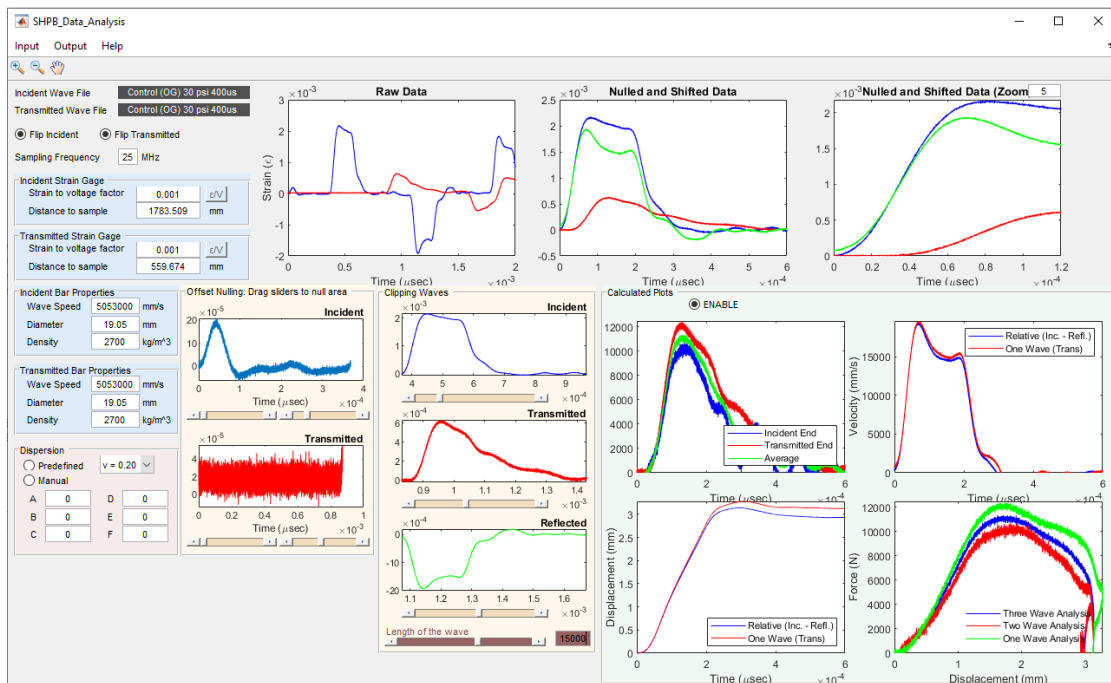


Figure 8 - MATLAB Primary Display Interface

To show that this is a closed system, the transmission wave should be equal to the reflected wave subtracted from the incident wave. In Figure 9 below, the top right and

bottom left plots show these two curves. Since they are relatively close to each other during the duration of the impact, the assumption holds that energy is conserved within the system.

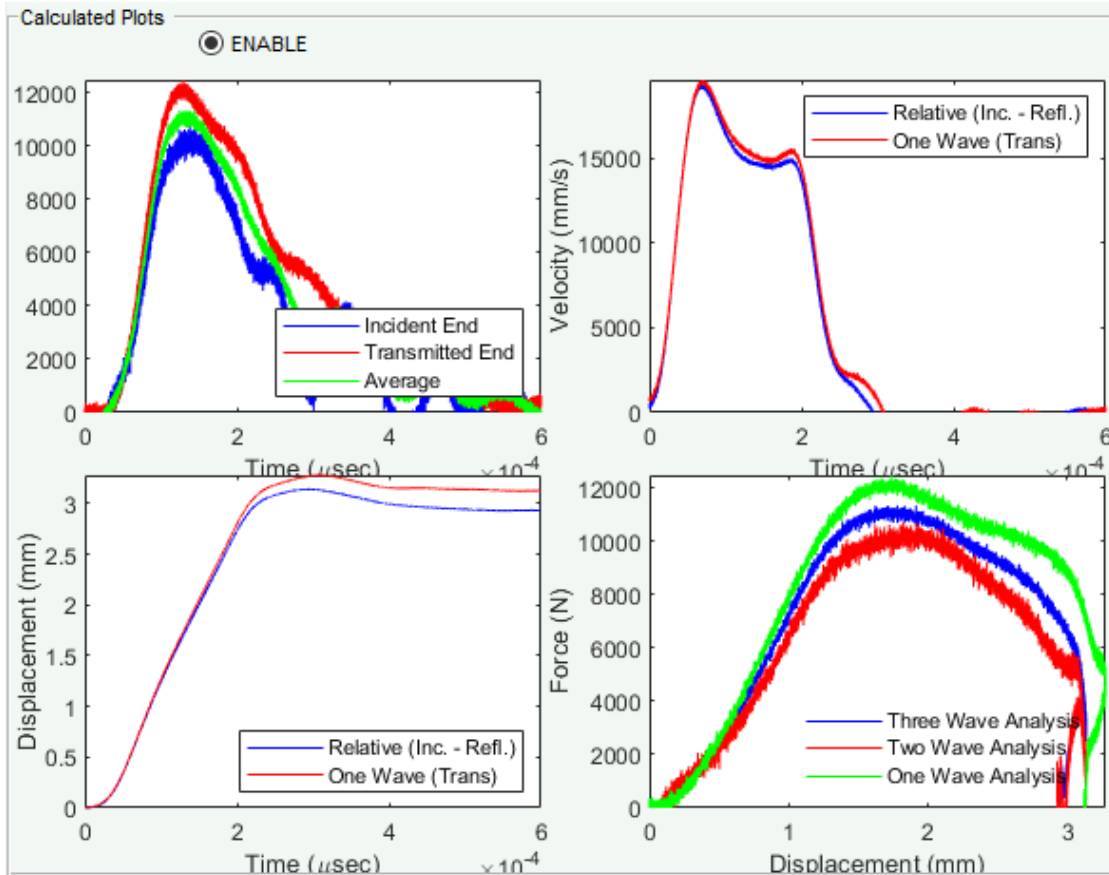


Figure 9 - Calculated Plots from Primary MATLAB Execution

Once complete, the MATLAB script was used to display the stress-strain results in Figure 10. Here, the compressive modulus can be determined, along with the stress, strain, and strain-rate of the sample. The data was exported into an excel document and the stress-strain curve plotted.

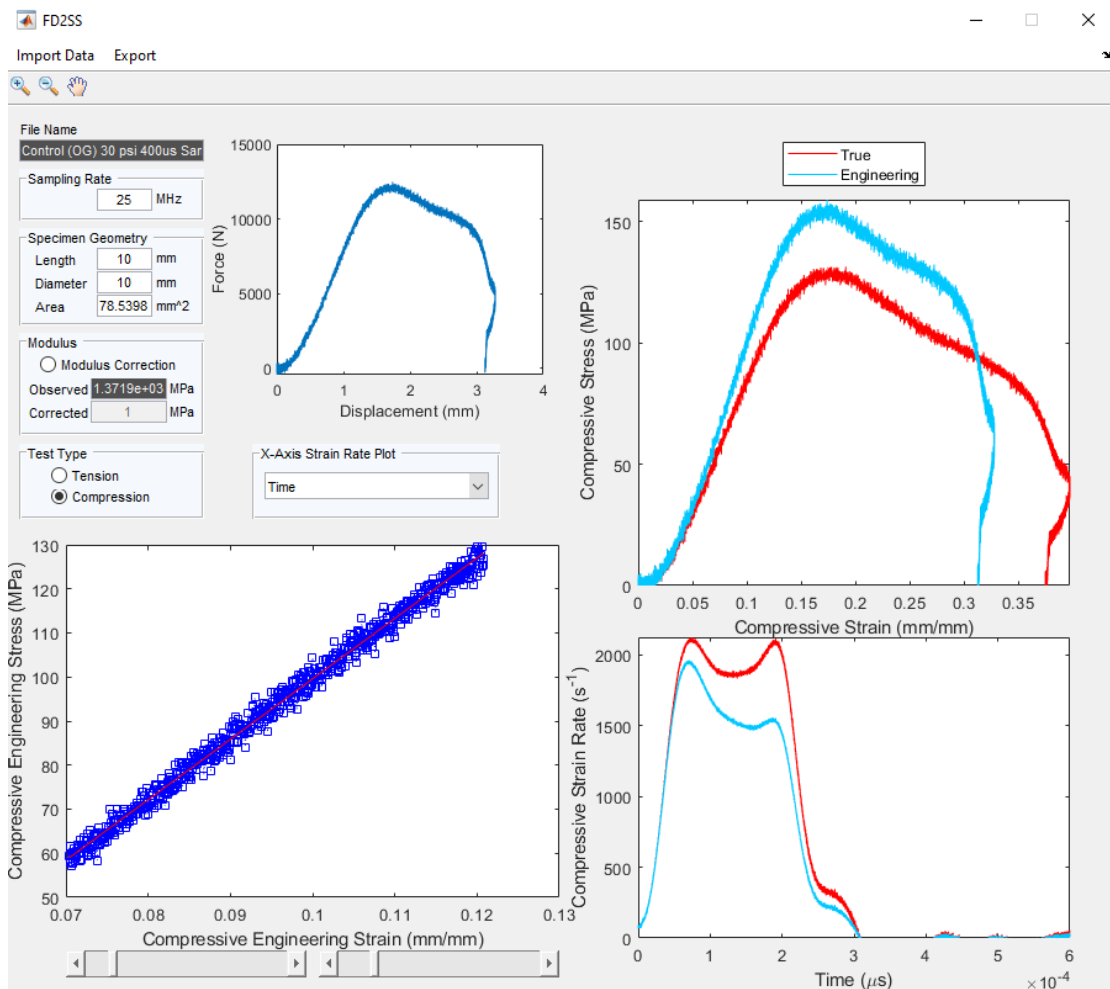


Figure 10 - MATLAB Final Display Interface

Digital Image Correlation Analysis

The purpose of using digital image correlation was to determine the strain in the sample over time to verify that they are similar to the strain-rate results from the MATLAB analysis. Figure 11 below shows the calibration of the video received from the camera. Using ProAnalyst software, since the diameter of the bar in the video is known to be 19.05 mm, this allows the software to determine the distance of each pixel in the video.

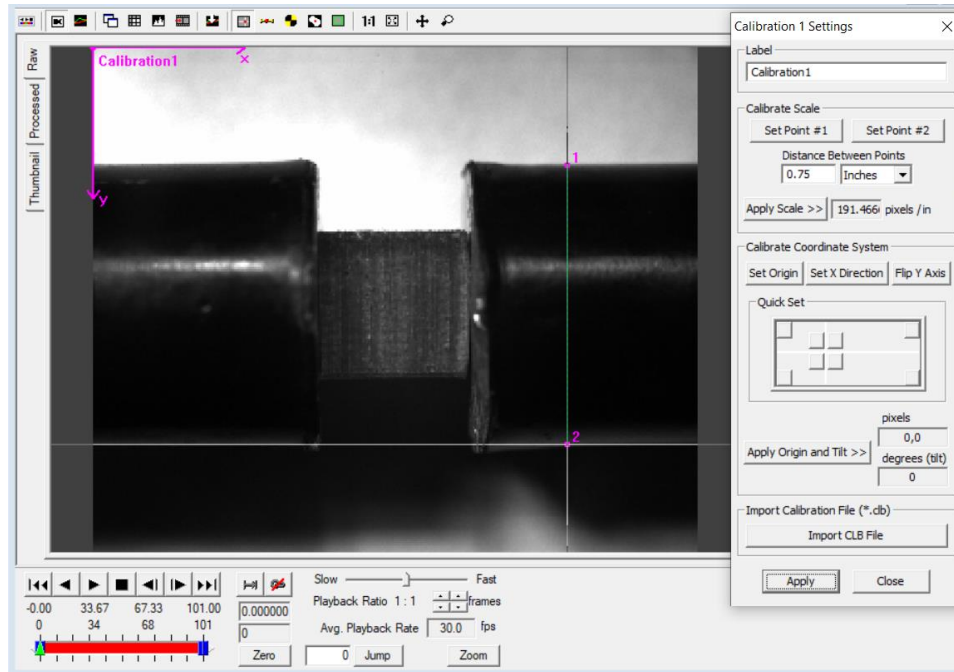


Figure 11 - ProAnalyst Calibration

Next, line tracking was enabled, allowing for edge tracking of the incident and transmission bar. The software tracks the edges of the incident bar and transmission bar, because that is the same as the length of the sample between the bars. Therefore, the software tracks the point on the end of each bar, which is where the video changes from black pixels to white pixels, which allows it to track the length of the sample as a function of time, which is shown below in Figure 12. This can be used to calculate the strain of the sample vs. time, which was plotted on a graph. Figures 13 through 18 show various examples of the strain vs. time plots for different samples tested. Each plot shows the strain vs. time as calculated using the DIC analysis and the data from the strain gauge that was calculated using MATLAB at each strain rate. These two curves being similar to each other verifies that the experimentally calculated stress and strain are accurate and reliable.

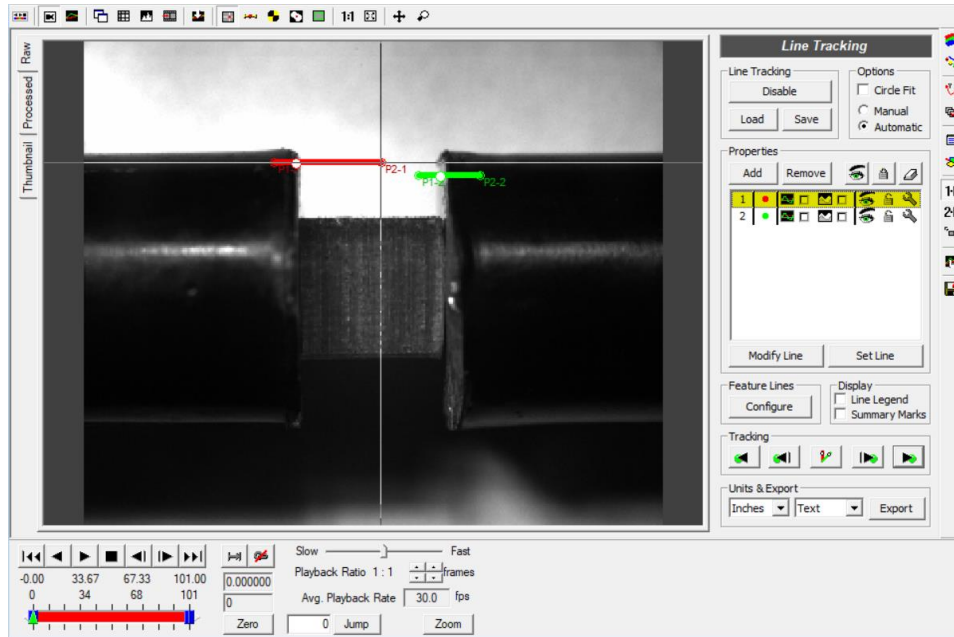


Figure 12 - ProAnalyst Line Tracking

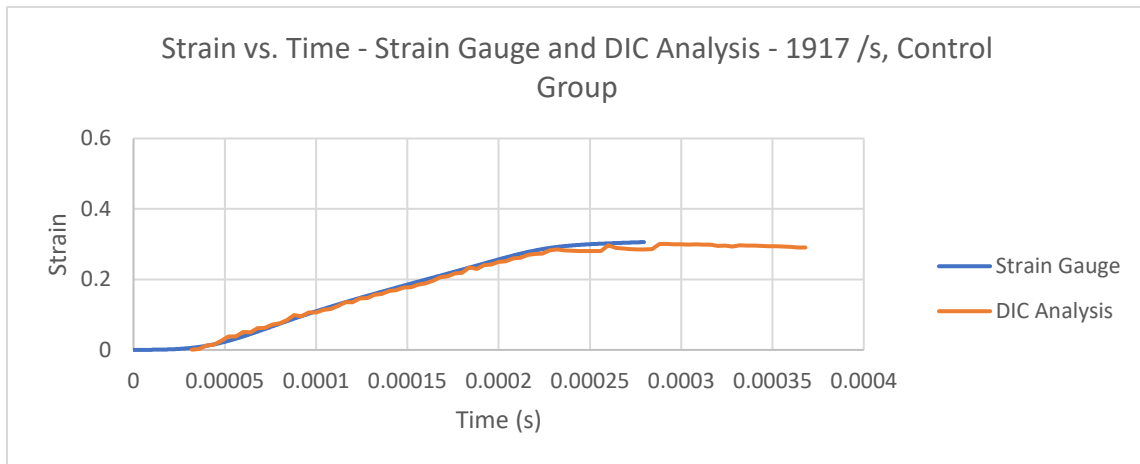


Figure 13 - Strain vs. Time - Strain Gauge/DIC Analysis – 1917 /s, Control Group

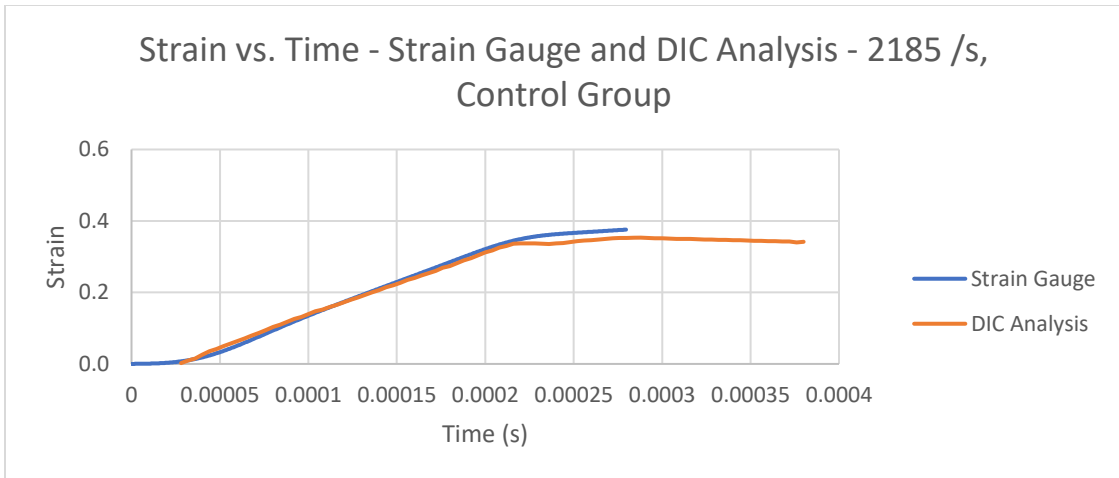


Figure 14 - Strain vs. Time - Strain Gauge and DIC Analysis – 2185 /s, Control Group

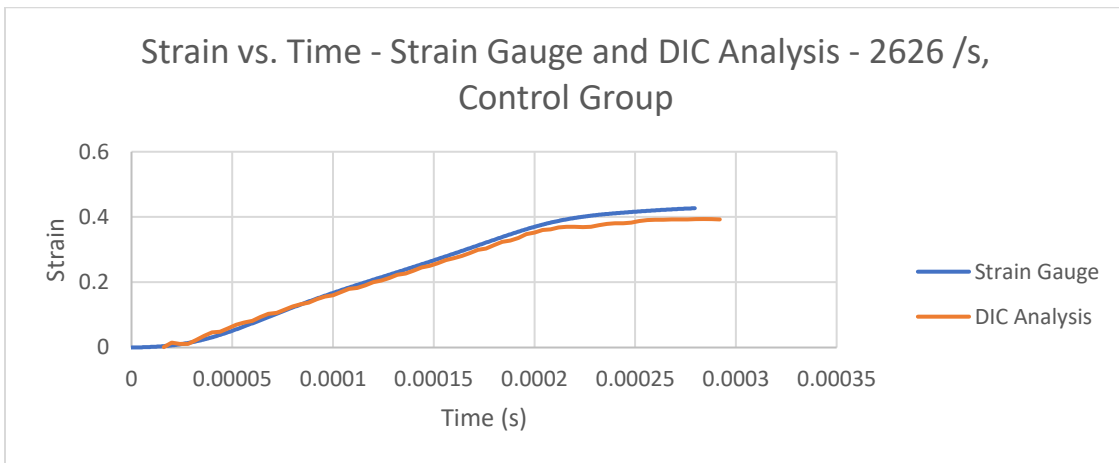


Figure 15 - Strain vs. Time - Strain Gauge and DIC Analysis – 2626 /s, Control Group

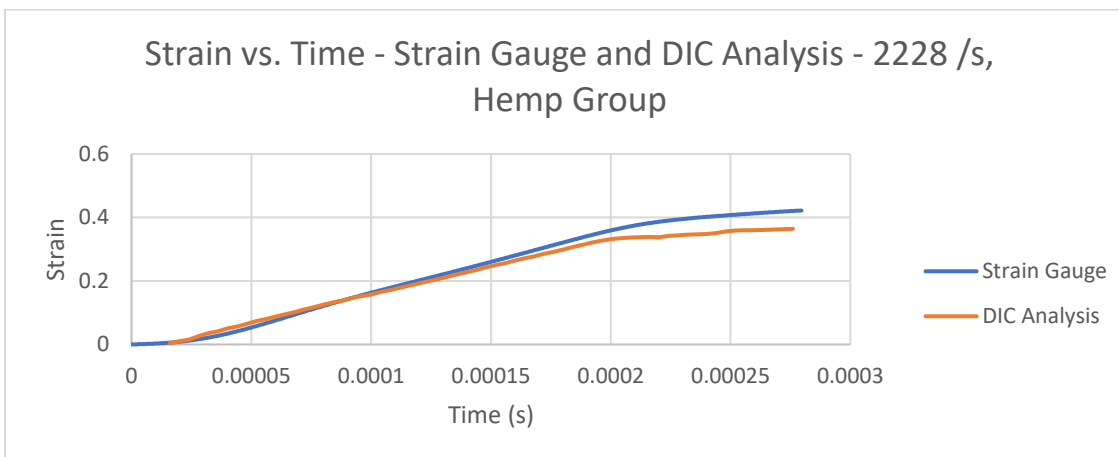


Figure 16 - Strain vs. Time - Strain Gauge and DIC Analysis – 2228 /s, Hemp Group

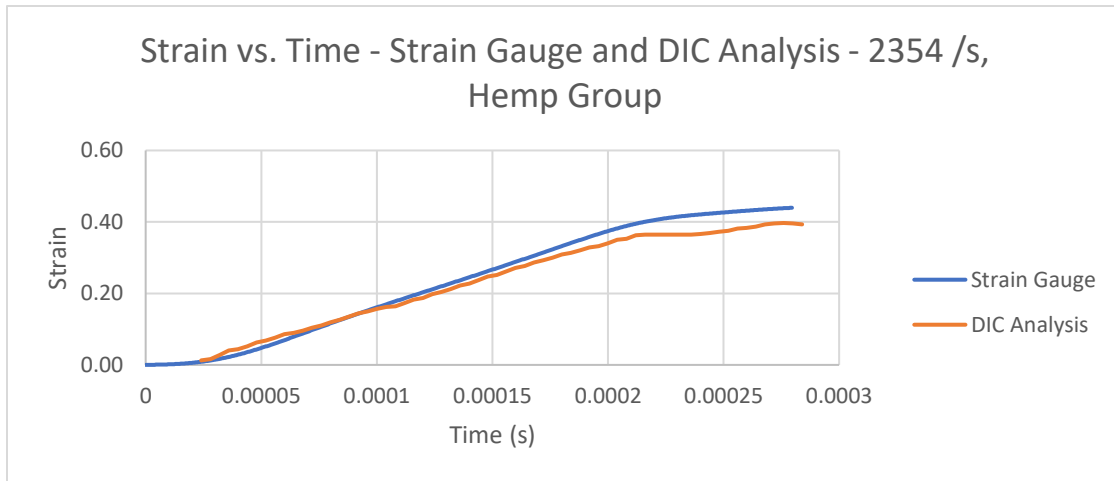


Figure 17 - Strain vs. Time - Strain Gauge and DIC Analysis – 2354 /s, Hemp Group

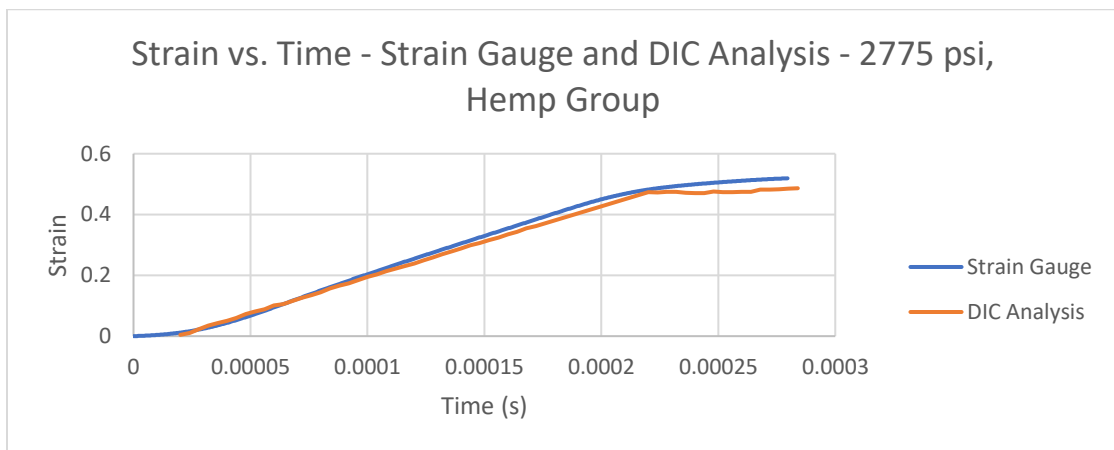


Figure 18 - Strain vs. Time - Strain Gauge and DIC Analysis – 2775 /s, Hemp Group

These six figures show that the strain of both materials under every different gas chamber pressure was measured accurately, because the curves from the strain gauge measurements and digital image correlation analysis are in agreement. Therefore, the results from this procedure using the data from the strain gauge can be considered accurate and reliable.

RESULTS AND DISCUSSION

Control PLA Group Results

Figure 19 below shows the nine control sample that were tested under strain-rates varying from 1821-2795 s^{-1} . The stress (MPa) as a function of strain (unitless) were plotted to show each sample's material properties under various high strain-rates.

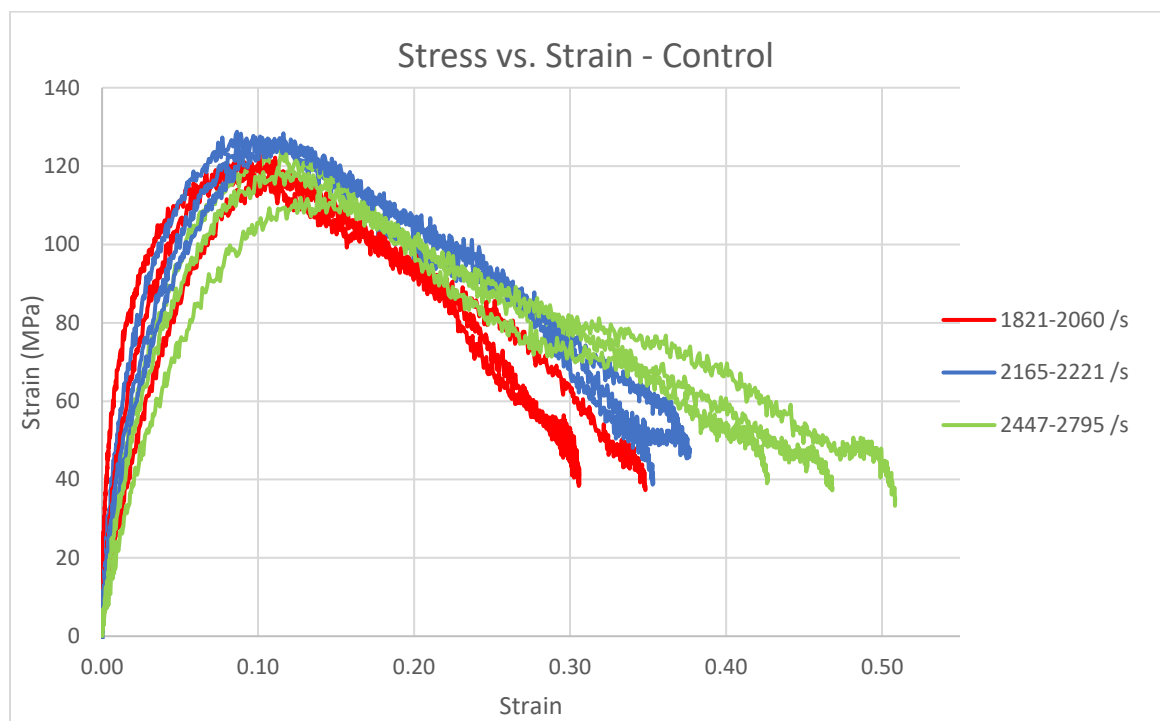


Figure 19 - Stress vs. Strain - Control Group

This figure shows all nine sample that were in the control group. Since there are so many lines on this plot that are close together, it is difficult to analyze. Therefore, it can be

broken up into three subplots which show the stress-strain curves of each set of three sample that were tested at the same gas chamber pressure. Figures 20 through 22 below show the stress-strain curves for the control group under 30, 40, and 50 pounds per square inch of pressure. The main explanation for the variation in these curves is the difference in pressure applied from the SHPB. The following three figures separate this plot into three subplots that represent the three pressures, which will make it easier to compare.

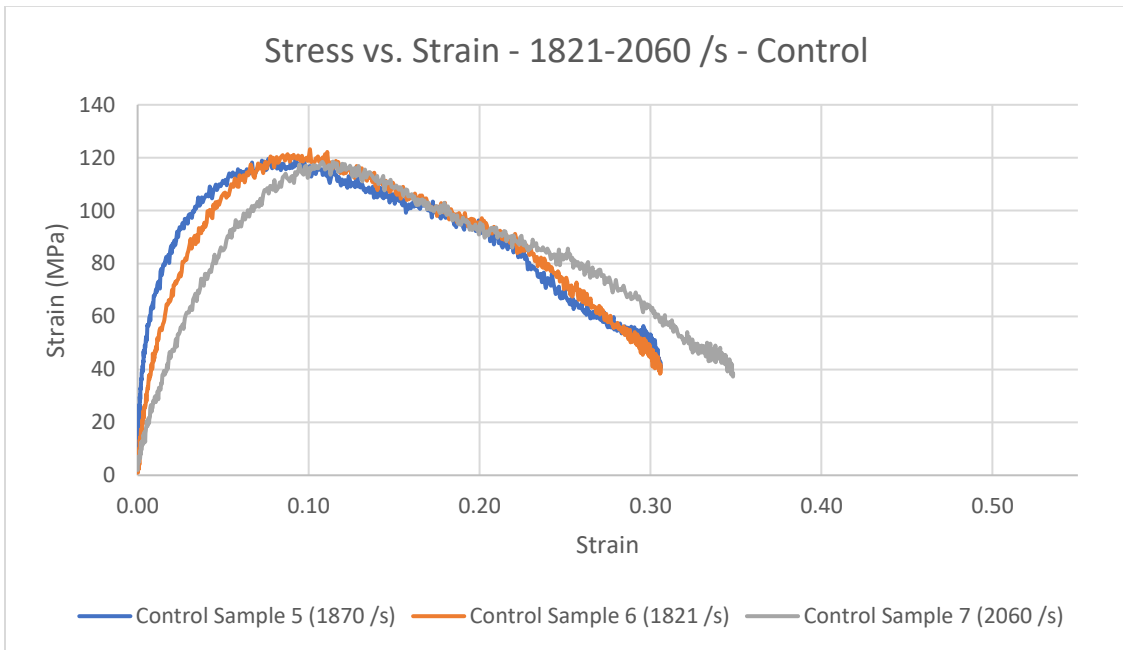


Figure 20 - Stress vs. Strain – 1821-2060 /s – Control

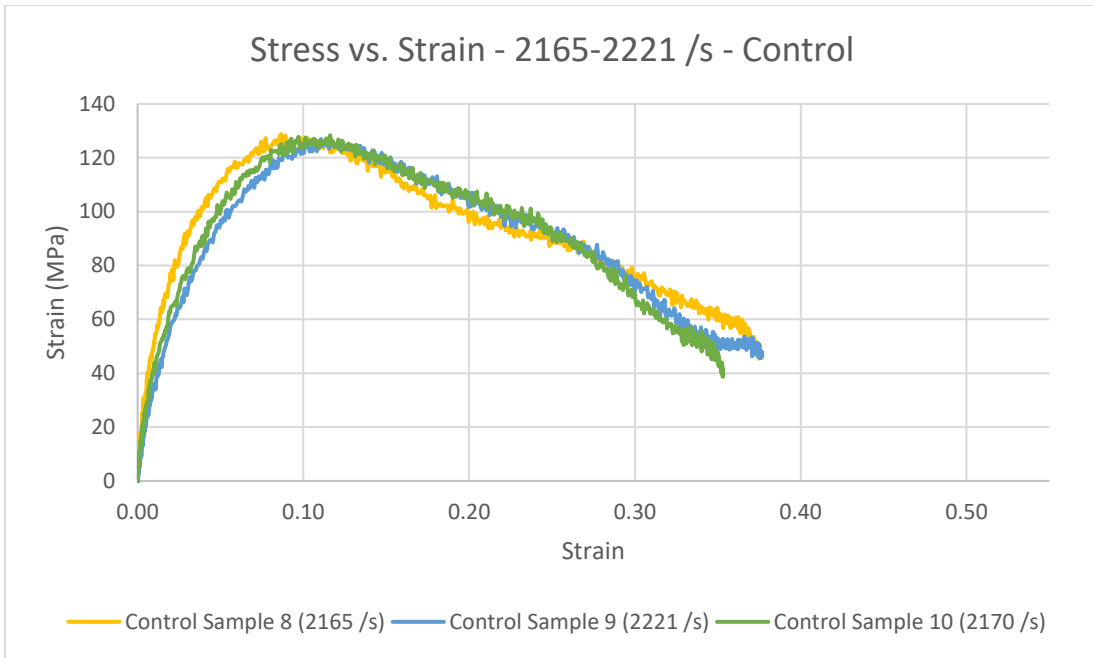


Figure 21 - Stress vs. Strain – 2165-2221 /s – Control

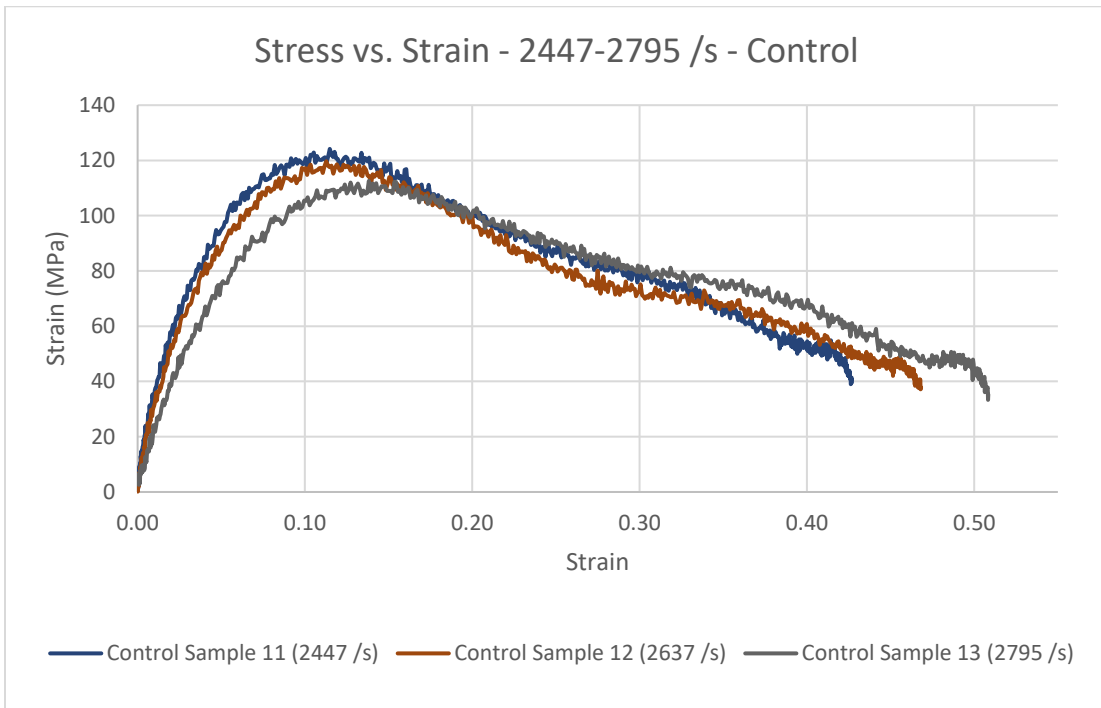


Figure 22 - Stress vs. Strain – 2447-2795 /s - Control

In each of the three figures, the strain-rates are similar, and the curves are close together. This shows that there is little variation in the response of the samples under similar strain rates.

Hemp-PLA Group Results

Figure 23 below shows the 9 hemp-PLA sample that were tested under strain-rates varying from 2125-2948 s^{-1} . The stress (MPa) as a function of strain (unitless) were plotted to show each sample's material properties under various high strain-rates.

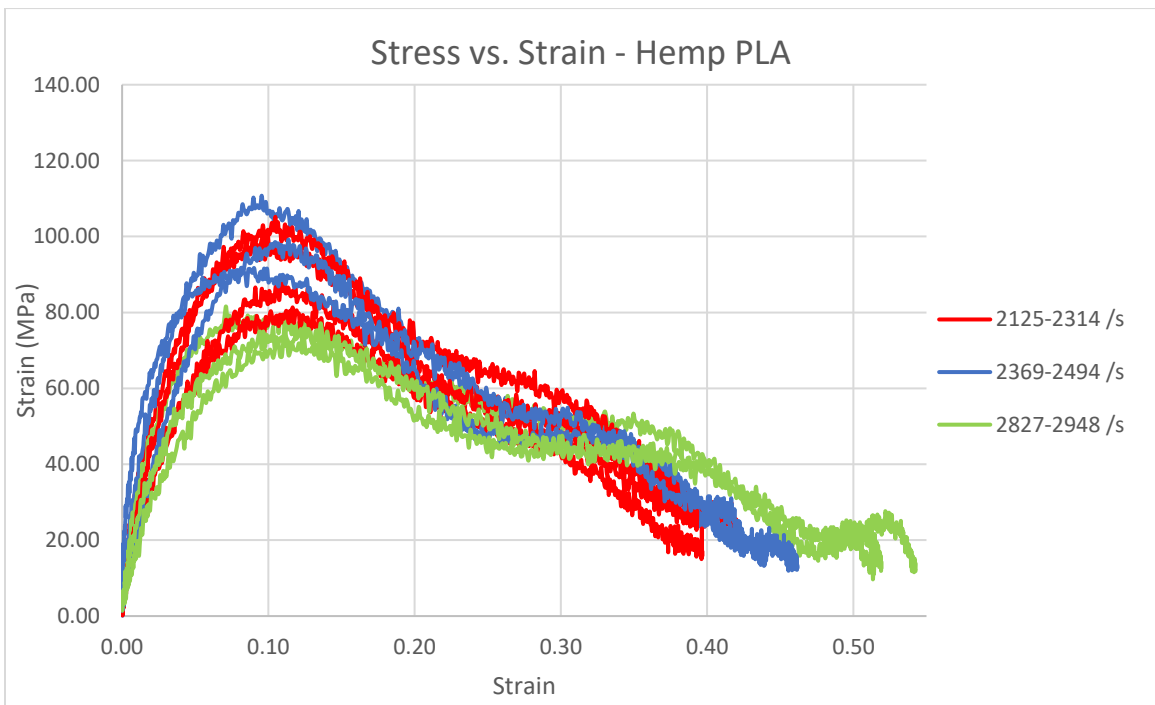


Figure 23 - Stress vs. Strain - Hemp-PLA Group

This figure shows all nine sample that were in the hemp-PLA group, split by color into three sections based on the strain-rate. The most likely cause of the variation in these

curves is the variation of the material due to the print. This plot was broken up into three subplots which show the stress-strain curves of each set of three sample that were tested at the same strain-rate, which are shown in Figures 24 through 26.

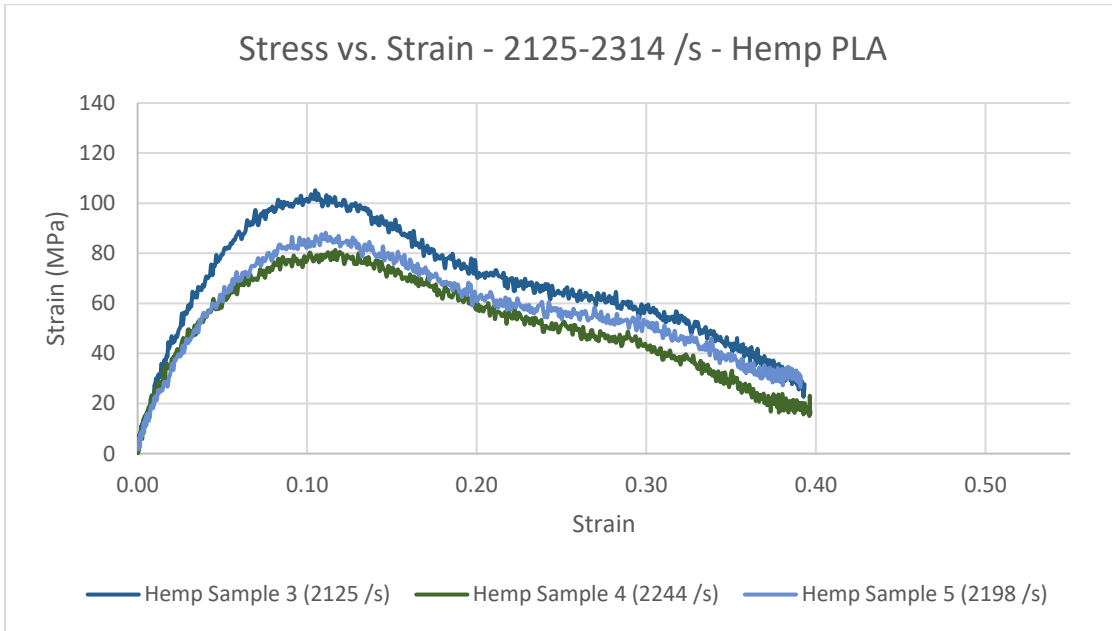


Figure 24 - Stress vs. Strain – 2125-2314 /s - Hemp PLA

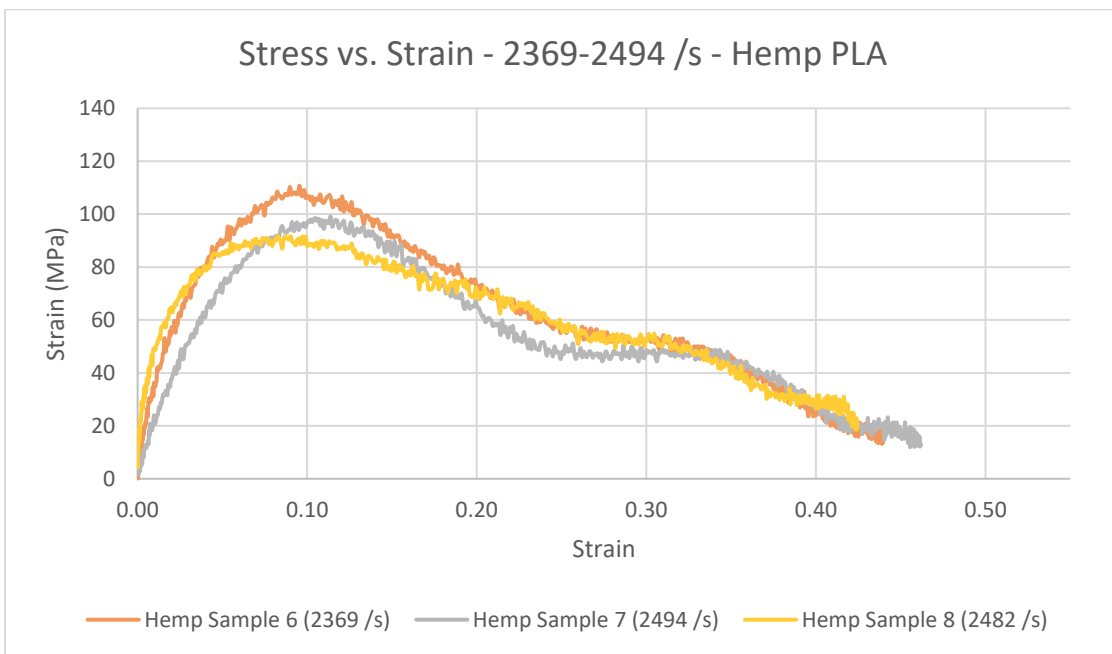


Figure 25 - Stress vs. Strain – 2369-2494 /s - Hemp PLA

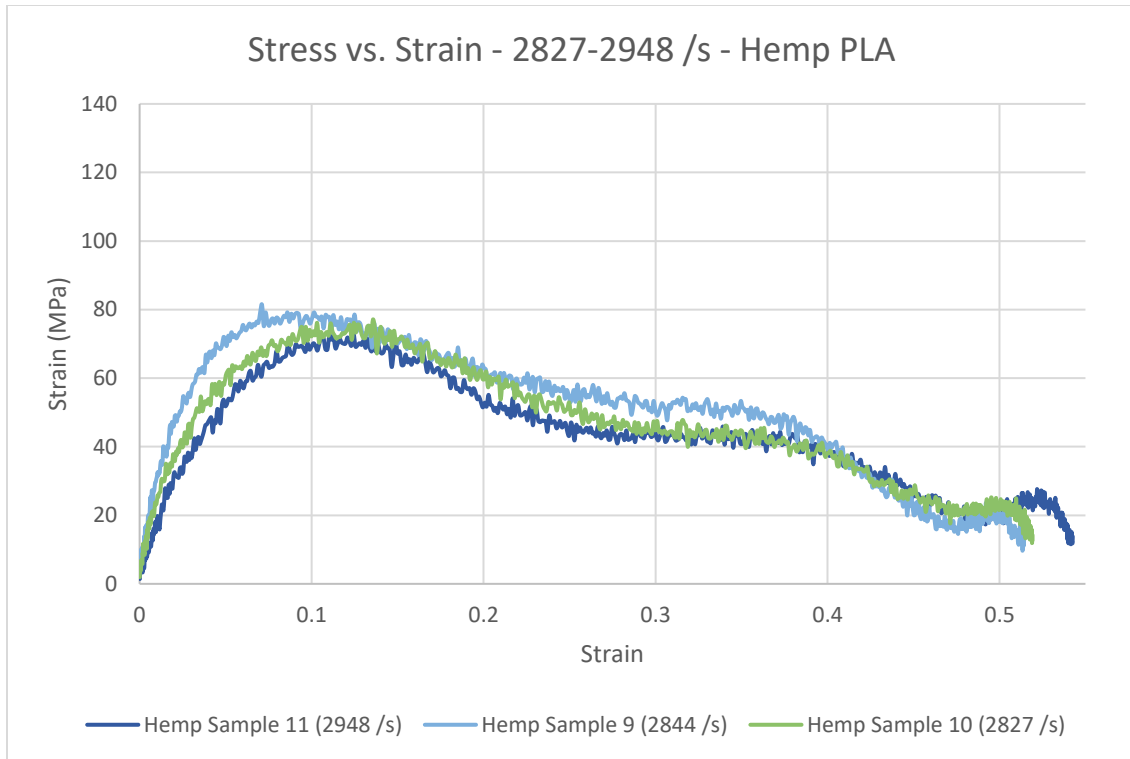


Figure 26 - Stress vs. Strain – 2827-2948 /s - Hemp PLA

As discussed previously for the control group, the three plots for the hemp samples can also be observed and analyzed marginally. There appears to be a higher variation of ultimate compressive strengths among the hemp group. Also, at similar strain rates, the graphs show that there is less energy density in the hemp samples than the control samples.

Comparisons

Figure 27 below shows the stress-strain curves of all samples in the control group (blue) and the hemp group (orange).

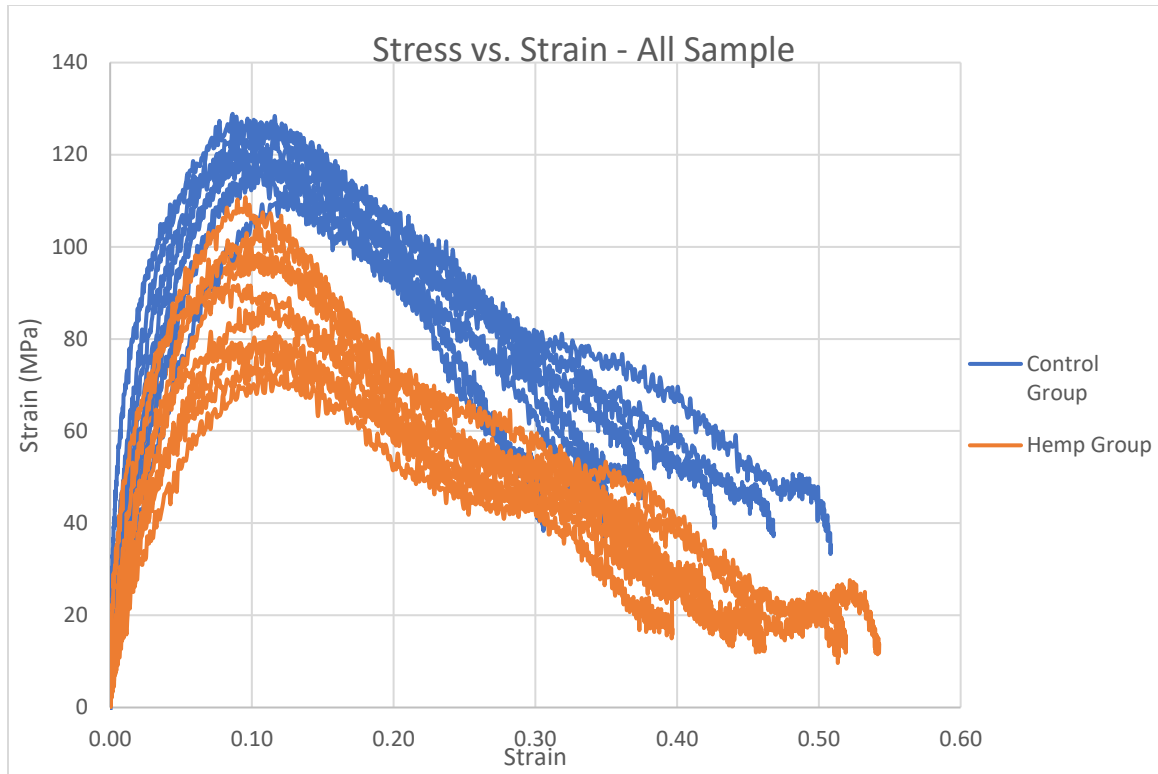


Figure 27 - Stress vs. Strain - Hemp (Orange) and Control (Blue)

Figure 28 below shows the ultimate compressive strength of each control and hemp sample as a function of the strain-rate. The ultimate compressive strength was determined by finding the maximum stress on the sample during the firing of the SHPB, and the strain-rate represents the maximum strain-rate calculated during compressive loading. The next figure, Figure 29, shows the ranges of the control and hemp samples based on the pressure of the SHPB gas chamber, and Figure 30 shows the overall range of compressive strength for each material.

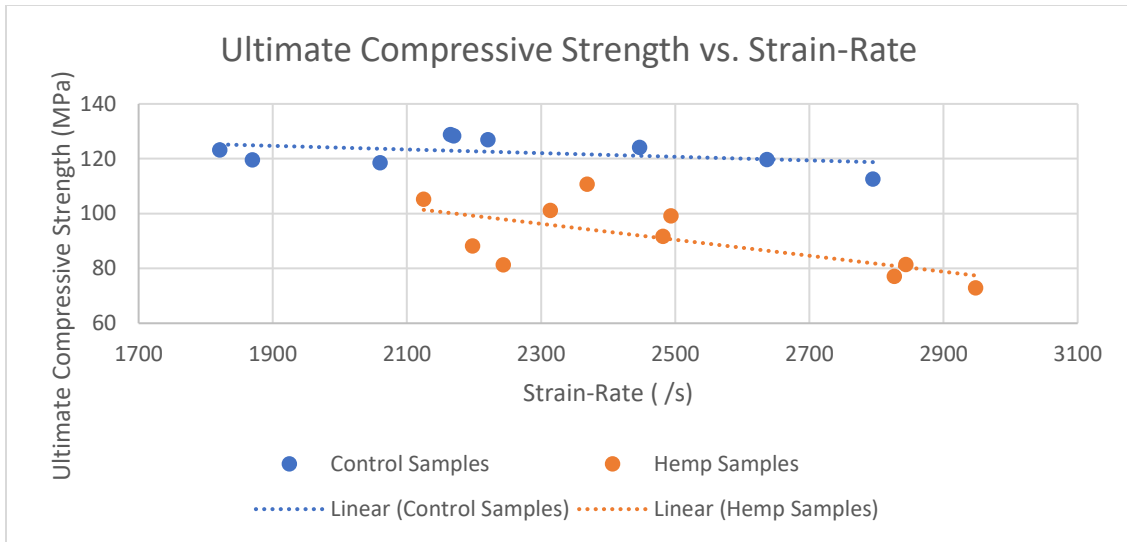


Figure 28 - Ultimate Compressive Strength vs. Strain-rate

The figure shows a decrease in the compressive strength of the hemp-fiber samples during the strain-rates tested, while the control samples show a flat line. This demonstrates that the hemp-fiber samples dropped in strength, while the control samples did not, in the range of strain-rates tested.

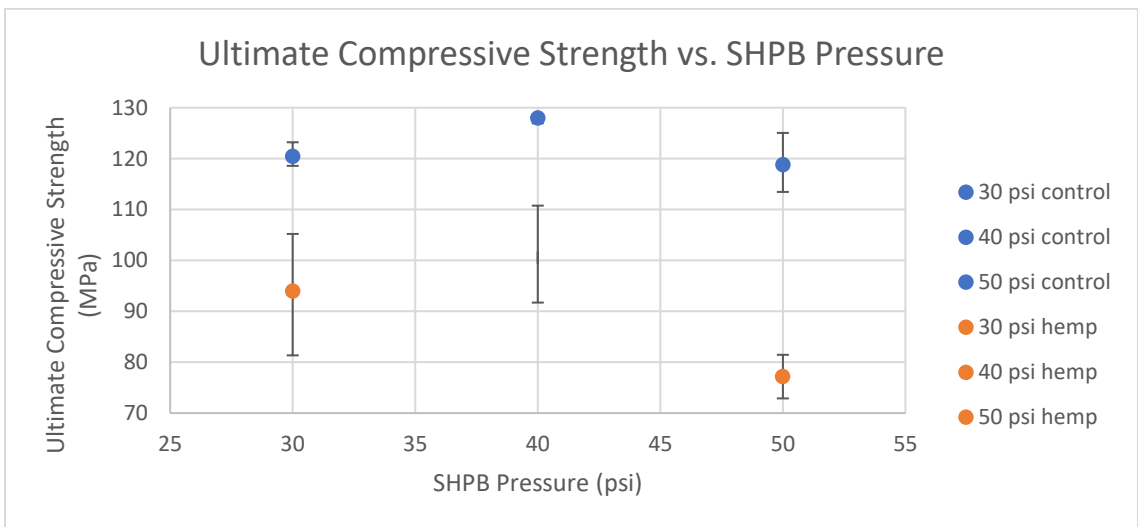


Figure 29 - Ultimate Compressive Strength vs. SHPB Pressure

This figure shows the drop in compressive strength of the hemp-fiber composites when the SHPB was at 50 psi, which was a strain rate between 2827 and 2948 /s. This is the only significant change in compressive strength in the hemp-fiber group, and there are no significant changes in compressive strength in the control group.

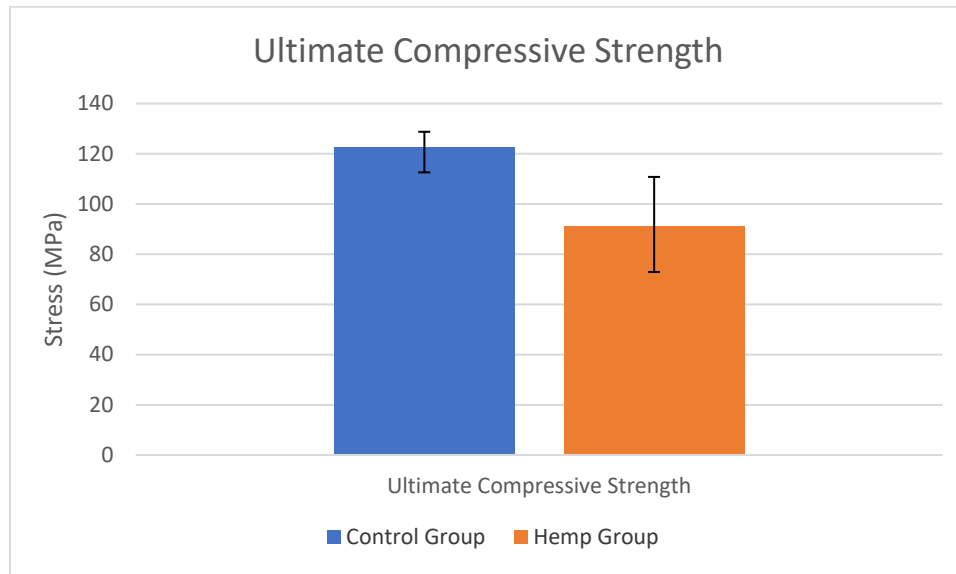


Figure 30 - Ultimate Compressive Strength

From Figure 28, the trendline makes it very easy to see the main difference in the ultimate compressive strength of the hemp group compared to the control group. Both materials show a gradual decrease in ultimate compressive strength as the strain-rate increases. Looking at Figure 29, the difference can also be seen, based off the pressure of the gas chamber in the SHPB. For each pressure, the control group displayed a higher compressive strength than the hemp group, even with the statistical spread. For both materials, there was a small increase in the compressive strength from 2100 to 2300 /s, but from 2300 to 2800 /s, there was a noticeable decrease in compressive strength of the hemp-fiber samples. Finally, Figure 30 shows that there was more variation in the compressive

strength of the hemp group than the control group, meaning the change in strain-rate had a greater effect on the hemp group than on the control group. Also, it is possible that the hemp fibers in the PLA that were perpendicular to the direction of the stress did not aid in the response of the composite. This would cause the fibers in the composite to act as empty space in the PLA, causing failure locations to occur.

The next three figures (31 through 33) show the comparison of the two materials' total specific energy in various displays. Figure 31 is a scatterplot with a linear trendline to show the general trend of each material's specific energy compared to the strain-rate, and Figure 32 shows the average total specific energies for each gas chamber pressure for each material tested, with the corresponding error shown. Finally, Figure 33 shows the average specific energy of the control and hemp group.

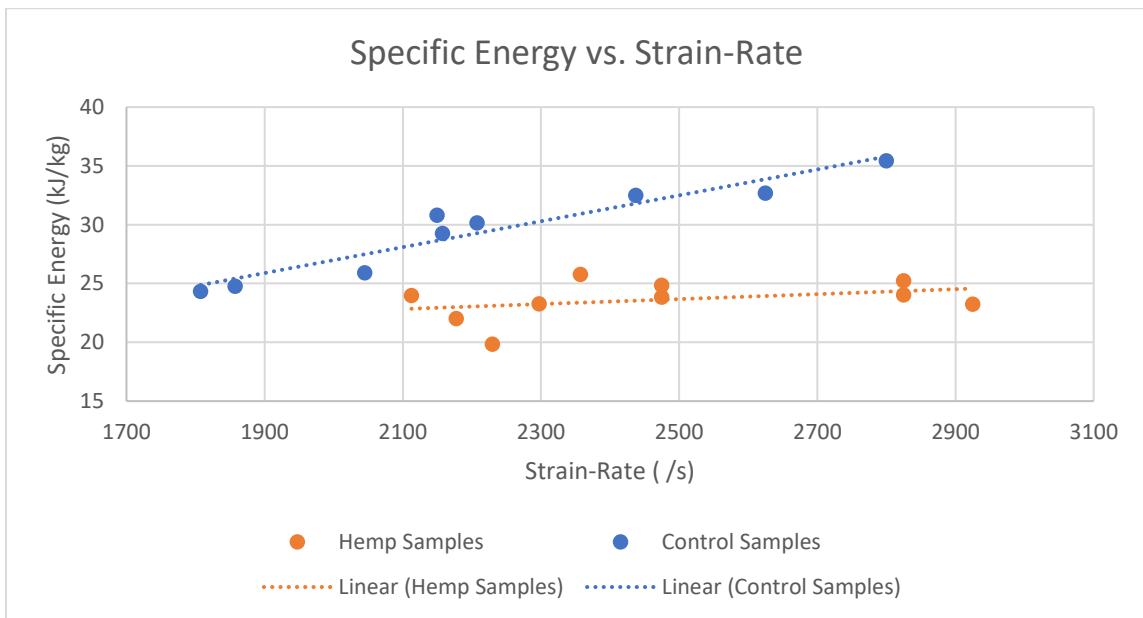


Figure 31 - Specific Energy vs. Strain-rate

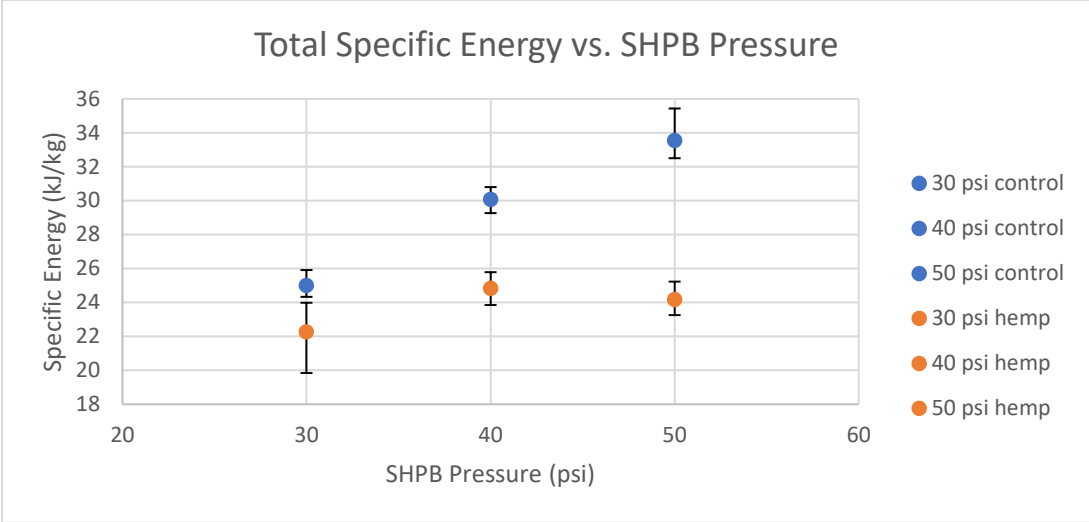


Figure 32 - Total Specific Energy vs. SHPB Pressure

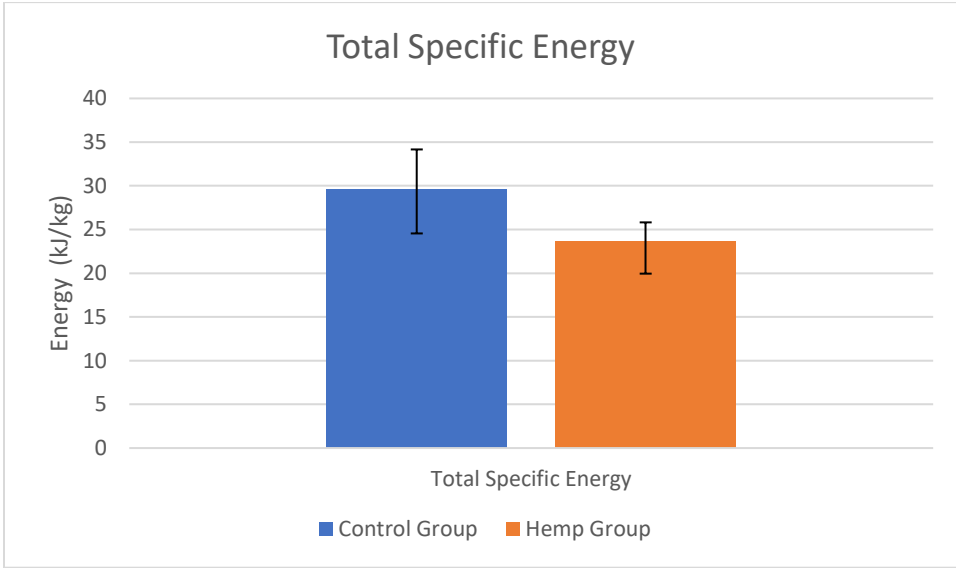


Figure 33 - Total Specific Energy

The specific energy represents how much energy the sample absorbed per unit mass during dynamic compression. Figures 31 and 32 both show that the specific energy of the control group was greater than the specific energy of the hemp group, based on both the strain of the sample and the pressure of the gas chamber of the SHPB. In addition, the

trendlines in Figure 31 suggest that the control group absorbs more energy as the strain-rate increases, while the hemp samples do not increase or decrease the amount of energy they absorb. This difference in specific energy may be due to the hemp fibers in the PLA that are perpendicular to the direction of stress, thus acting as empty space in the PLA. This causes the fibers to absorb less energy than if PLA were in its place, causing the specific energy of the composite to be smaller than the specific energy of the pure PLA.

Figures 34 through 37 below show the same representation of energy absorbed by the samples; however, they show the damage initiation energy and damage propagation energy of the samples. This helps to get a clearer understanding of how and when the two materials absorbed energy. This is important because the damage initiation energy is useful in applications where failure is not desired, whereas damage propagation energy is more useful when the material should absorb as much energy as possible, even if that means it must go past the failure point.

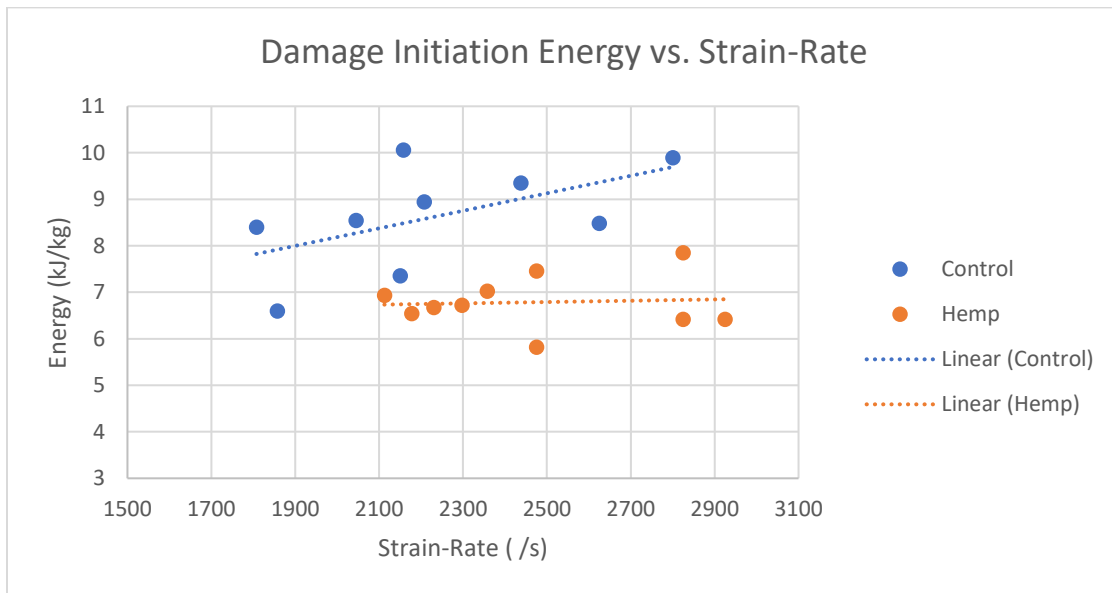


Figure 34 - Damage Initiation Energy vs. Strain-rate

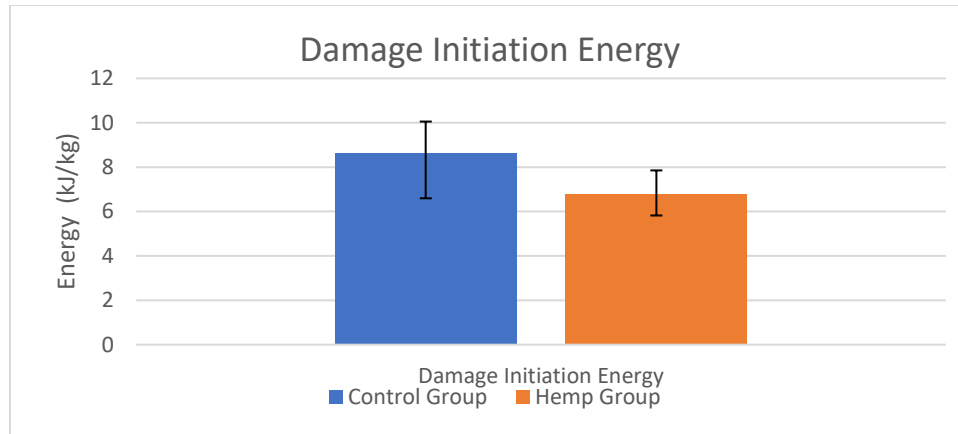


Figure 35 - Damage Initiation Energy

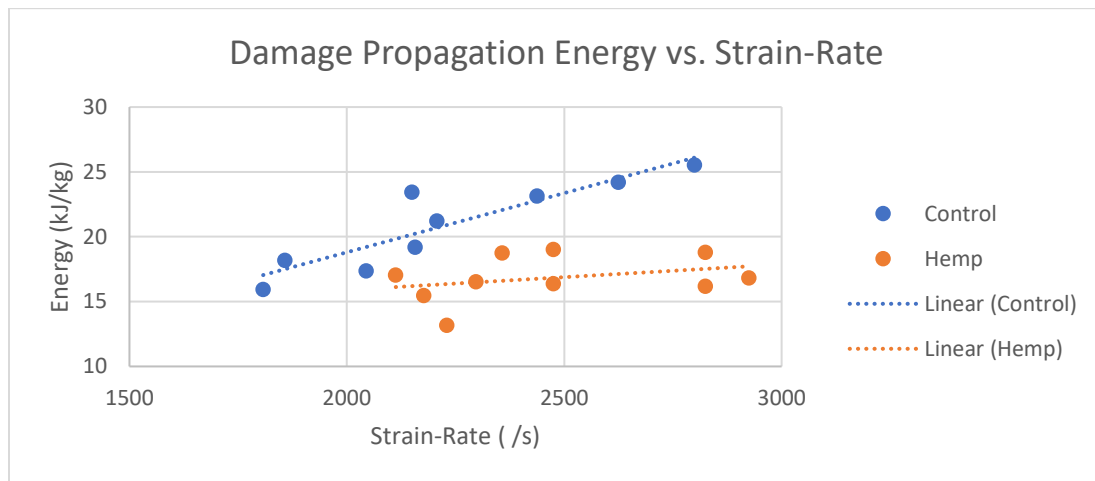


Figure 36 - Damage Propagation Energy vs. Strain-rate

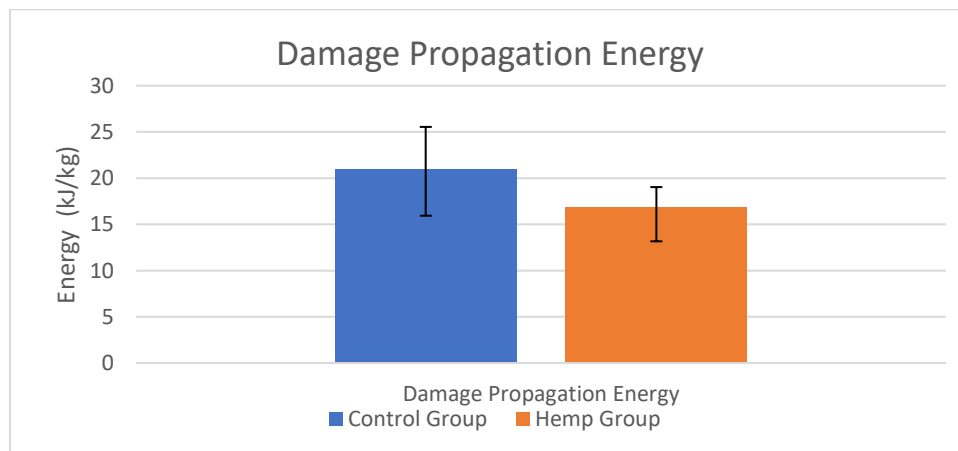


Figure 37 - Damage Propagation Energy

Looking at the damage initiation and damage propagation energy, the trends are very similar. There is very little increase in energy absorbed by the hemp samples as the strain-rate increases, while the energy absorbed by the control group increases as the strain-rate increases. Both components of the specific energy are similar to the trends of the specific energy. This is likely because there is no impact of the fiber on when failure occurs compared to when the PLA fails. Therefore, the fibers do not influence when the PLA fails in the range of strain rates tested. Also, looking at the trendlines in Figures 34 and 36, the damage initiation and damage propagation energies tend to be larger in the control samples for a given strain-rate than the hemp composites. This is likely a result of the fibers not aiding the PLA in the response to compressive loading, since they are not oriented parallel to the direction of the stress. This would cause a decrease in the energy absorbed by the hemp-fiber PLA composite before and after failure.

Table 1 below shows the ranges of the strain-rate, ultimate compressive strength, damage initiation, damage propagation, and total specific energy of the two materials.

Table 1 - Ranges of Main Results - Control vs. Hemp-PLA

	PLA Control Group	Hemp-PLA Group
Strain-rate (s^{-1})	1807-2800	2112-2925
Ultimate Compressive Strength (MPa)	112.5-128.8	72.8-110.8
Specific Energy (kJ/kg)	24.3-35.4	19.84-25.2
Damage Initiation Energy (kJ/kg)	6.60-10.06	6.42-7.85
Damage Propagation Energy (kJ/kg)	15.93-25.54	13.17-19.04

The compressive strength of the hemp group ranged from 72.8 to 110.8 MPa. The former compressive strength was 35% smaller than the control group minimum compressive strength, and the latter compressive strength was 14% smaller than the control group maximum compressive strength. Since the hemp samples had smaller compressive strengths, it means they were not able to resist stress as effectively as the control samples.

The amount of energy absorbed by the impact on the sample is the other important factor for analyzing the material's reaction to a high strain-rate. The total specific energy of the hemp samples ranged from 19.84 to 25.2 kJ/kg, while the control group ranged from 24.3 to 35.4 kJ/kg. Between the minimum and maximum values of the hemp group, the minimum value is 18% smaller than that of the control group, and the maximum value of the hemp group is 29% smaller than that of the control group. The damage initiation energy of the hemp samples ranged from 6.42 to 7.85 kJ/kg, while the control group ranged from 6.60 to 10.06 kJ/kg. The minimum value of the hemp group was just 3% smaller than that of the control group, and the maximum value was 28% smaller than that of the control group. This suggests that for the lower strain-rates, there was less variation in damage initiation energy, but when the strain-rate increased, the control group was able to absorb more energy before failure than the hemp group. This could also be seen in Figure 34, where the trendline for the damage initiation energy of the hemp samples showed a flat line, while the trendline for the control group showed an increase in energy as the strain-rate increased. The damage propagation energy of the hemp group ranged from 13.17 to 19.04 kJ/kg, while the control group ranged from 15.93 to 25.54 kJ/kg, meaning the hemp was 17% and 25% less than the control group minimum and maximum values, respectively. Based on this data, it appears that the hemp group showed lower energy absorption after

failure (damage propagation) than the control group. However, the hemp showed more similar energy absorption before failure (damage initiation) for lower strain-rates, but when the strain-rate increased, the gap appeared again between the two groups, and the hemp group absorbed significantly less energy than the control group. There was a decrease in both specific energy and compressive strength of the hemp group compared to the control group.

The hemp fibers are introduced into the PLA filament, which acts as a resin that holds the fibers together. The fibers are only beneficial in a composite when they contribute to the material's resistance to tension or compression. If the fibers are not aiding in the response, they decrease the dynamic properties because they are replacing resin that would be contributing to the material's resistance to tension and compression. Fibers are much more likely to resist tension or compression when the fibers are parallel to the direction of the stress. The hemp fibers in the samples tested in this procedure were not oriented in any specific direction; they are miniscule fibers in random orientations. In addition, when the filament is melted during the additive manufacturing process of 3D-printing, the fibers were not set in any special orientation. This makes it much more likely that the hemp fibers in the PLA filament is the reason there is a deficit in the performance of the hemp-PLA in comparison to the 100% PLA.

The other part of the performance of the hemp-PLA that can be explained is the damage initiation results being more similar when the pressure was 30 psi, but the damage initiation of the control group increasing as the pressure increased, while this did not happen for the hemp-PLA group. Under the lower strain-rates in this procedure, the hemp fibers may have had greater contribution to the material's resistance to compression, but

when the strain-rate increased, the hemp fibers were not able to resist the compression as well as the pure PLA, so the hemp did not perform as well as the control group.

CONCLUSIONS

The conclusions from this procedure are summarized below.

- As the strain rate increased from 2100 /s to 2900 /s, the hemp-fiber PLA composites showed a decrease in compressive strength, while the control group showed no change in compressive strength.
- As the strain rate increased from 2100 /s to 2900 /s, the hemp-fiber PLA composite showed no change in specific energy, while the control group showed an increase in specific energy. The damage initiation and damage propagation of each material exhibited similar trends.

LIST OF REFERENCES

- [1] Fazita, M. & H.P.S, Abdul Khalil & Ayob, Nor & Rizal, Samsul. (2019). Effects of strain rate on failure mechanisms and energy absorption in polymer composites. 10.1016/B978-0-08-102293-1.00003-6.
- [2] Hemp is the Future of Plastics. Ali Asghar Modi, Rehmatullah Shahid, Muhammad Usman Saeed, Tanzila Younas.
- [3] Entwined v2 Hemp, 1.75 mm Natural / 1kg 1.75 mm Spool / Entwined Hemp Filled PLA. 3-D Fuel. Retrieved March 22, 2022, from <https://www.3dfuel.com/products/entwined-hemp-filament-1-75mm?variant=12773385830512>.
- [4] Duval, Antoine & Bourmaud, Alain & Augier, Laurent & Baley, Christophe. (2011). Influence of the sampling area of the stem on the mechanical properties of hemp fibers. *Materials Letters*. 65. 797-800. 10.1016/j.matlet.2010.11.053. https://www.researchgate.net/publication/233537351_Influence_of_the_sampling_area_of_the_stem_on_the_mechanical_properties_of_hemp_fibers
- [5] Chaudhry, S, Al-Dojayli, M, & Czekanski, A. "Performance of 3-D Printed Thermoplastic Polyurethane Under Quasi-Static and High-Strain Rate Loading." Proceedings of the ASME 2016 International Mechanical Engineering Congress and Exposition. Volume 9: Mechanics of Solids, Structures and Fluids; NDE,

Diagnosis, and Prognosis. Phoenix, Arizona, USA. November 11–17, 2016. V009T12A065. ASME. <https://doi.org/10.1115/IMECE2016-67839>

[7] Ravi Kiran Chintapalli, Stephanie Breton, Ahmad Khayer Dastjerdi, Francois Barthelat, Strain rate hardening: A hidden but critical mechanism for biological composites? *Acta Biomaterialia*, Volume 10, Issue 12, 2014, Pages 5064-5073, ISSN 1742-7061, <https://doi.org/10.1016/j.actbio.2014.08.027>.

[8] Khieng TK, Debnath S, Ting Chaw Liang E, Anwar M, Pramanik A, Basak AK. A Review on Mechanical Properties of Natural Fibre Reinforced Polymer Composites under Various Strain Rates. *Journal of Composites Science*. 2021; 5(5):130. <https://doi.org/10.3390/jcs5050130>

[9] High strain-rate behavior of natural fiber-reinforced polymer composites <https://journals.sagepub.com/doi/abs/10.1177/0021998311414946?journalCode=jcma>

[10] Dezi, Francesca & Gara, Fabrizio & Roia, Davide. (2016). Dynamic Characterization of Open-ended Pipe Piles in Marine Environment. 10.5772/62055.

[11] <https://www.relinc.com/wp-content/uploads/2014/07/SHPB-Equations-used-in-SURE-Pulse.pdfanaly>